https://doi.org/10.5194/gmd-2023-214
Preprint. Discussion started: 21 November 2023

Geoscientific Model Development Discussions
Open Access
EGU

Implementation and evaluation of diabatic advection in the Lagrangian transport model MPTRAC 2.6

Jan Clemens[1,2,3], Lars Hoffmann[2,3], Bärbel Vogel[1,3], Sabine Grießbach[2,3], and Nicole Thomas[1,3]

[1]Institut für Energie- und Klimaforschung (IEK-7), Forschungszentrum Jülich, Jülich, Germany
[2]Jülich Supercomputing Centre (JSC), Forschungszentrum Jülich, Jülich, Germany
[3]Center for Advanced Simulation and Analytics (CASA), Forschungszentrum Jülich, Jülich, Germany

Correspondence: j.clemens@fz-juelich.de

Abstract.

Diabatic transport schemes with hybrid zeta coordinates, which follow isentropes in the stratosphere, are known to greatly improve Lagrangian transport calculations compared to the kinematic approach. However, some Lagrangian transport calculations with a diabatic approach, such as the Chemical Lagrangian Transport Model of the Atmosphere (CLaMS), show low computational performance on modern high-performance computing (HPC) architectures. Here, we implemented and evaluated a new diabatic transport scheme in the Massive-Parallel Trajectory Calculations (MPTRAC) model. While MPTRAC effectively exploits modern HPC architectures, it was previously limited to kinematic trajectories on pressure coordinates. The extended modelling approach now enables the use of either kinematic or diabatic vertical velocities and the coupling of different MPTRAC modules based on pressure or hybrid zeta coordinates.

The evaluation of the new transport scheme in MPTRAC shows that after 90-day forward calculations distributions of air parcels in the upper troposphere and lower stratosphere (UTLS) are almost identical for MPTRAC and CLaMS. No significant bias between the two Lagrangian models was found. Furthermore, after one day, internal uncertainties (e. g., due to interpolation or the numerical integration method) in the Lagrangian transport calculations are at least one order of magnitude smaller than external uncertainties (e. g., from reanalysis selection or downsampling of ERA5). Differences between trajectories using either CLaMS or MPTRAC are on the order of the combined internal uncertainties within MPTRAC. Since the largest systematic differences are caused by the reanalysis and the vertical velocity (diabatic vs. kinematic) the results support the development efforts for trajectory codes that can access the full resolution of ERA5 in combination with diabatic vertical velocities. This work is part of a larger effort to adapt Lagrangian transport in state-of-the-art models such as CLaMS and MPTRAC to current and future HPC architectures and exascale applications.

1 Introduction

The Massive-Parallel Trajectory Calculations (MPTRAC) model is a Lagrangian transport model that was developed to efficiently run on modern HPC architectures, which often rely on GPUs (Hoffmann et al., 2019, 2022). The MPTRAC model aims to improve upon the advection schemes of state-of-the-art Lagrangian transport models, which have potentially, even with traditional code adaption strategies, limited capability to fully leverage the opportunities offered by recent HPC architectures

https://doi.org/10.5194/gmd-2023-214
Preprint. Discussion started: 21 November 2023

Geoscientific Model Development Discussions

(Bauer et al., 2021). One such state-of-the-art Lagrangian transport model is the Chemical Lagrangian Transport Model of the Stratosphere (CLaMS) trajectory module (McKenna et al., 2002a, b).

However, unlike MPTRAC, CLaMS can be used with diabatic vertical velocities and a hybrid vertical coordinate (referred to as hybrid zeta coordinate or zeta coordinate). Diabatic vertical velocities are calculated from radiative balance instead of the mass balance as in the case of kinematic vertical velocities. The hybrid zeta coordinate was first introduced by Mahowald et al. (2002) and later implemented into CLaMS by Konopka et al. (2004). It corresponds to an orography-following sigma coordinate at the ground and a quasi-horizontal potential temperature coordinate at levels above around 380 K (Pommrich et al., 2014). This combination of hybrid zeta coordinates and diabatic velocities significantly improves Lagrangian transport simulations and trajectory calculations, especially in the stratosphere (e.g. Eluszkiewicz et al., 2000; Ploeger et al., 2010b, 2011; Schoeberl and Dessler, 2011; Brinkop and Jöckel, 2019; Li et al., 2020). The improvements result from the fact that the flow in the stratosphere is mostly isentropic and the vertical transport is closely linked to diabatic heating rates.

Earlier versions of MPTRAC were formulated in pressure coordinates only and ran with kinematic vertical velocities (Hoffmann et al., 2019, 2022). Following the approach of CLaMS, we newly implemented an advection scheme for MPTRAC to run with diabatic vertical velocities in hybrid zeta coordinates. In addition to the approach in CLaMS, MPTRAC's advection scheme is formulated to be compatible with other modules of MPTRAC that remain operating on pressure coordinates. Thus, in MPTRAC, advection can be performed with the diabatic scheme as in CLaMS, while modules based on pressure coordinates, such as the particle diffusion or convection module, can be used in a coupled mode. The implementation of the diabatic scheme in MPTRAC also improves the interoperability between the MPTRAC trajectory module and the global 3-dimensional CLaMS version, including i.a. irreversible mixing or chemistry calculations (McKenna et al., 2002b; Pommrich et al., 2014; Vogel et al., 2019; Ploeger et al., 2021).

Uncertainty sources of Lagrangian transport models have been studied extensively in the past (e.g. Stohl, 1998; Stohl et al., 2001; Bowman et al., 2013). Uncertainty sources in transport simulations can be distinguished into external and internal sources. External uncertainties are related to the data driving the model, e.g. to the reanalysis used, differences between reanalysis products and the limited resolution of the wind data. Internal uncertainties are the necessary elements of the transport model, e.g. interpolation, integration methods or the handling of model boundaries at the surface. To evaluate the newly implemented diabatic transport scheme in MPTRAC, we investigated the differences in trajectory calculations caused by the use of MPTRAC compared to CLaMS. To put the differences found in the trajectory calculations between CLaMS and MPTRAC in a broader context, the effects of, first, external sources (using different reanalyses in different resolutions or different vertical velocities) and, second, internal sources (e.g. interpolation and integration methods) were investigated.

External uncertainties of Lagrangian transport simulations due to differences between the used wind data are discussed frequently (e.g. Stohl et al., 2004; Angevine et al., 2014; Hoffmann et al., 2019; Li et al., 2020; Ploeger et al., 2021; Vogel et al., 2023b). First of all, limited resolution of the reanalysis fields itself creates a limitation for the accuracy of the transport calculations because sub-grid scale processes are not accounted for without parameterisation (e.g. Rolph and Draxler, 1990). The stochastic parameterisations that are required to account for unresolved sub-grid scale winds and turbulent diffusion impose an uncertainty to the transport as well. Second, reanalysis fields show systematic differences because of different dynamical cores,

https://doi.org/10.5194/gmd-2023-214
Preprint. Discussion started: 21 November 2023

Geoscientific Model Development Discussions

assimilation processes, resolution and parameterisations if compared with each other. Hoffmann et al. (2019) showed that systematic differences due to the chosen reanalysis (comparing ERA5 and ERA-Interim) are larger than transport deviations due to parameterized sub-grid scale diffusion in *kinematic* transport calculations. Angevine et al. (2014) found for a limited case (using FLEXPART-WRF in the troposphere) that the uncertainty in a WRF ensemble propagates into CO tracer mixing ratio uncertainties of about 30% to 40%. Furthermore, Stohl et al. (2004) noted that inconsistencies of reanalysis data, which are caused by separate assimilation cycles, lead to artificial diffusion in Lagrangian transport calculations. Therefore, quantities such as potential vorticity (PV) or potential temperature are less conserved than physically expected. These inconsistencies are however absent in forecast data and might depend on the assimilation method of a selected reanalysis. In summary, systematic differences of the reanalyses and their underlying models are expected to be a major source of external uncertainty for Lagrangian transport simulations, followed by processes that are not included in the reanalysis data (e.g. unresolved sub-grid scale processes).

Internal uncertainties related to different integration methods applied in MPTRAC have been investigated by Rößler et al. (2018). They found that the Euler method has about one order of magnitude higher error growth rates in comparison to the mid-point scheme in the stratosphere. However, the mid-point scheme is only two to four times less accurate than third and fourth order Runge-Kutta schemes, with no significant differences between the third and fourth order schemes. Rößler et al. (2018) attribute the latter to the errors related to linear interpolation of the meteorological data that limits benefits of higher order integration methods such as the fourth order Runge-Kutta scheme. Interpolation errors, if higher order integration is applied, could be the main internal source of error for deviations between Lagrangian transport models. Uncertainties as a consequence of interpolation have also been discussed in more detail by Stohl et al. (1995, 2001). Their results suggest interpolation and the integration scheme as the leading internal sources of uncertainty.

Differences between transport models have been studied as well. Differences in transport using different Lagrangian models (MPTRAC, ClaMS) driven by *kinematic* vertical velocities are smaller than differences caused by parameterised sub-grid scale winds and turbulent diffusion (Hoffmann et al., 2019). Stohl et al. (2001) concluded, based on a comparison of three trajectory models, that the selection of the data is more important than the selection of the model for accuracy. In the literature (see also Stohl et al., 2001; Bowman et al., 2013), meteorological data are consequently considered the main source of uncertainty in Lagrangian transport simulations, while internal model differences, mainly due to interpolation and integration methods, are usually much smaller. Here, we validate these findings for the two most recent ECMWF reanalysis ERA-Interim and ERA5 with CLaMS and MPTRAC.

To justify that MPTRAC and CLaMS trajectory calculations can mutually substitute each other, the MPTRAC and CLaMS model do not to need to be bit-identical but deviations must be much smaller than from external uncertainty sources, e.g. reanalysis differences, vertical velocities and sub-grid scale diffusion and on the order of combined internal uncertainties. In our study we show that after implementing hybrid zeta coordinates and diabatic vertical velocities in MPTRAC, MPTRAC and CLaMS results of forward-trajectory calculations differ only insignificantly. CLaMS and MPTRAC trajectory calculations can substitute each other, which bears a path forward for combined CLaMS-MPTRAC simulations on upcoming HPC systems.

https://doi.org/10.5194/gmd-2023-214
Preprint. Discussion started: 21 November 2023


Geoscientific Model Development Discussions

Further, we quantify and order in more detail the sources of transport uncertainties that are found in Lagrangian models and the driving data.

In chapter 2 we introduce the trajectory models and the used reanalyses. Afterwards, differences between CLaMS and MPTRAC are described. Subsequently, the diagnostics used to compare the different model results and to assess the source of uncertainties are presented. In chapter 3 the model differences are evaluated, starting from case studies, going to a comparison between trajectories after one day, and ending with a long-term simulation of particle distributions. Finally, our conclusion is presented, that differences between CLaMS and MPTRAC trajectory calculations (as a consequence of internal sources) are negligible in comparison to the variability of the results caused by external sources such as different reanalysis or vertical velocities.

2 Methods and data

Diabatic transport calculations in hybrid zeta coordinates were implemented in MPTRAC, similar to CLaMS. Lagrangian transport calculations rely on, first the Lagrangian transport model itself and second, the input wind fields that drive the model. In the following sections the implementation of diabatic transport into MPTRAC and CLaMS, the used meteorological data as well as the used diagnostic to evaluate diabatic transport in MPTRAC are described in detail.

2.1 Lagrangian transport models

CLaMS is a comprehensive chemical Lagrangian transport model, including i.a. irreversible mixing and stratospheric chemistry (McKenna et al., 2002a, b; Pommrich et al., 2014; Konopka et al., 2022). Here, we focus on the advection scheme of CLaMS as a reference for the implementation of a similar advection scheme in MPTRAC. MPTRAC is a Lagrangian transport model that contains, among others, modules for advection and the parameterisation of diffusion from sub-grid scale winds and turbulence (Hoffmann et al., 2022). Trajectory calculations with both models are used in many studies, mostly focusing on UTLS and stratospheric transport processes (most recently Liu et al., 2023; Clemens et al., 2023; Vogel et al., 2023a). The implementation of diabatic transport in hybrid-coordinates, i.e. of a diabatic transport scheme into MPTRAC has four essential components: the choice of the height coordinate (hybrid zeta coordinate instead of pressure), the vertical velocity (diabatic instead of kinematic), the interpolation method, and the integration method (Runge-Kutta or mid-point). These aspects will be further discussed below.

2.1.1 Vertical coordinates

CLaMS applies the vertical hybrid zeta coordinate (ζ) with associated diabatic vertical velocity $\dot{\zeta} = \frac{d\zeta}{dt}$ for trajectory calculations (Mahowald et al., 2002; Konopka et al., 2004; Pommrich et al., 2014). For this study, this scheme was implemented in MPTRAC as well. The hybrid zeta coordinate is defined as shown in Eq. (1)

https://doi.org/10.5194/gmd-2023-214
Preprint. Discussion started: 21 November 2023

Geoscientific Model Development Discussions
Open Access
EGU

$$\zeta(p) = \begin{cases} \theta(p,T) & \text{if}\, \sigma < \sigma_r \\ \theta(p,T) \sin\left(\frac{1-\sigma(p)}{1-\sigma_r}\right) & \text{if}\, \sigma \geq \sigma_r \end{cases} \tag{1}$$

where p is the pressure and p_s denotes the local surface pressure. $\sigma = \frac{p}{p_s}$ is called sigma coordinate and σ_r is a reference level in sigma coordinates. $\theta(p,T)$ is the potential temperature. Near the surface, the hybrid zeta coordinate follows the orography in the form of a sigma-like coordinate. At higher altitudes, starting from the reference level ($\sigma_r = 0.3$), the zeta coordinate is smoothly transformed into the potential temperature $\theta(p,T)$. The reference level $\sigma_r = 0.3$ corresponds to a pressure around 300 hPa (≈ 380 K) depending on the local surface pressure.

Equation (2) shows that the time derivative of the hybrid zeta coordinate is the time derivative of the potential temperature, the diabatic ascent rate respectively, at altitudes above the reference level σ_r. At lower levels, the transport is a combination of diabatic rates $\dot{\theta}$ and kinematic rates $\dot{\sigma}$ (Mahowald et al., 2002; Konopka et al., 2004). The diabatic and kinematic rates are taken from reanalysis data. While the diabatic rates are derived from radiative transfer calculations (Ploeger et al., 2021), kinematic rates are calculated from the continuity equation.

$$\dot{\zeta}(p) = \begin{cases} \dot{\theta}(p,T) & \text{if}\, \sigma < \sigma_r \\ \dot{\theta}(p,T) \sin\left(\frac{1-\sigma(p)}{1-\sigma_r}\right) + \theta(p,T) \cos\left(\frac{1-\sigma(p)}{1-\sigma_r}\right) \frac{1-\dot{\sigma}(p)}{1-\sigma_r} & \text{if}\, \sigma \geq \sigma_r \end{cases} \tag{2}$$

The diabatic approach in hybrid zeta coordinates greatly improves transport in the UTLS and stratosphere, where transport is mostly isentropic or affected by much lower diabatic heating rates in the vertical direction. In addition, mixing often occurs quasi-horizontally on isentropic surfaces, making this coordinate ideal for application in the stratosphere.

However, the diabatic approach also has disadvantages, such as the need to smooth zeta profiles that are not monotonic with height, that many processes in the troposphere are not diabatic (e.g. convection) and that parameterisations developed for pressure coordinates are not accessible and would have to be reformulated. In our new implementation of diabatic vertical velocities into MPTRAC, we avoid the latter by performing the calculation of advection in zeta coordinates, but transforming the zeta coordinates to pressure coordinates after advection, and vice versa from pressure to zeta coordinates before advection. In this way, other modules of MPTRAC (diffusion, convection, sedimentation, etc.) can still operate with pressure as the vertical coordinate, for which they were originally developed.

2.1.2 Numerical integration scheme

To compute Lagrangian trajectories, the ordinary differential equation $\frac{\mathrm{d}\boldsymbol{x}(t)}{\mathrm{dt}} = \boldsymbol{V}(t,\boldsymbol{x})$ has to be solved. The wind field $\boldsymbol{V}(t,\boldsymbol{x}) = (u, v, \dot{\zeta})$ is given on a discrete, spatio-temporal grid, provided by the reanalysis. The equation is solved using the classical fourth order Runge-Kutta method in CLaMS. In MPTRAC, both the mid-point scheme as well as the fourth-order Runge-Kutta method can be used (Rößler et al., 2018).

https://doi.org/10.5194/gmd-2023-214
Preprint. Discussion started: 21 November 2023

Geoscientific Model Development Discussions
Open Access
EGU

For an integration time step $t_{i+1} = t_i + dt$ (where dt can be lower than the temporal resolution of the data) the Runge-Kutta method is defined with the Equations (3) to (4).

$$\boldsymbol{x_{i+1}} = \boldsymbol{x_i} + \frac{1}{6}\left(\boldsymbol{k_1} + 2\boldsymbol{k_2} + 2\boldsymbol{k_3} + \boldsymbol{k_4}\right) dt \tag{3}$$

$$\boldsymbol{k_1} = \boldsymbol{V}(t_i, x_i) \quad \boldsymbol{k_2} = \boldsymbol{V}\left(t_i + \frac{dt}{2}, \boldsymbol{x_i} + dt\,\frac{\boldsymbol{k_1}}{2}\right) \quad \boldsymbol{k_3} = \boldsymbol{V}\left(t_i + \frac{dt}{2}, \boldsymbol{x_i} + dt\,\frac{\boldsymbol{k_2}}{2}\right) \quad \boldsymbol{k_4} = \boldsymbol{V}\left(t_i + dt, \boldsymbol{x_i} + dt\,\boldsymbol{k_3}\right) \tag{4}$$

The mid-point scheme, which is a second order Runge-Kutta scheme, is defined by Eq. (5).

$$\boldsymbol{x}_{i+1} = \boldsymbol{x}_i + dt\,\boldsymbol{V}\left(t_i + \frac{dt}{2}, \boldsymbol{x_i} + \frac{dt}{2}\boldsymbol{V}(t_i, \boldsymbol{x}_i)\right) \tag{5}$$

While, the Runge-Kutta method has fifths order truncation error ($\mathcal{O}(dt^5)$) and a fourth order accumulated error ($\mathcal{O}(dt^4)$), the mid-point scheme has third order ($\mathcal{O}(dt^3)$) truncation error and a second order accumulated error ($\mathcal{O}(dt^2)$) (Rößler et al., 2018).

2.1.3 Interpolation

During the integration time steps, the horizontal wind and vertical velocity must be interpolated to the air parcel locations. For the Runge-Kutta method, wind fields must be interpolated four times to the given time, horizontal location, and zeta height. For the mid-point scheme, this is reduced to two interpolations. For MPTRAC and CLaMS four-dimensional linear interpolation methods are performed, which are common for Lagrangian transport models (Bowman et al., 2013). However, the specific details of the interpolation in CLaMS and MPTRAC differ because the wind fields are not regularly provided in hybrid zeta coordinates, but in hybrid eta coordinates as applied in ECMWF's Integrated Forecasting System (Simmons et al., 1989). Interpolation with positions given only in zeta coordinates therefore requires additional considerations. In addition, MPTRAC has modules that rely on a formulation in pressure coordinates, requiring frequent conversions from pressure to zeta and vice versa. Finally, time interpolation is performed locally for each air parcel in MPTRAC. In contrast, CLaMS interpolates the wind field globally in advance for the four time steps of the Runge-Kutta scheme.

Figure 1 illustrates the interpolation as implemented in CLaMS (which is also referred to as interpolation "V0"). Let ζ_{ijkl} be the zeta coordinate and Q_{ijkl} a quantity which is supposed to be interpolated to the position of the air parcel. Both, the coordinate and the quantity are required to be formulated in a hybrid eta coordinate. In detail, the indices i, j, k refer to the indices on the three dimensional grid in longitude λ_i, latitude ϕ_j and the vertical hybrid eta coordinate η_k. The index l refers to the time t_l. Furthermore, let $(\lambda_{\mathrm{AP}}, \phi_{\mathrm{AP}}, \zeta_{\mathrm{AP}}, t_{\mathrm{AP}})$ be the position and time of the air parcel to which the quantity Q_{ijkl} needs to be interpolated. At the beginning of the interpolation in CLaMS, the interpolation in time is performed. For this purpose the neighbouring times t_0 and t_1 are selected so that $t_0 \leq t_{\mathrm{AP}} < t_1$ (see Fig. 1 (1)). With the data from the neighbouring times a linear interpolation of ζ_{ijkl} and Q_{ijkl} is done to the time t_{AP} (2). This provides three dimensional fields ζ_{ijk} and Q_{ijk} (3). Then, the

https://doi.org/10.5194/gmd-2023-214
Preprint. Discussion started: 21 November 2023

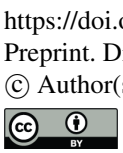

Geoscientific Model Development Discussions

horizontal indices of the air parcel are determined $(i_{\mathrm{AP}}, j_{\mathrm{AP}})$ using the horizontal coordinates λ_{AP} and ϕ_{AP} and the horizontal grid of longitudes λ_i and latitudes ϕ_j (4). The indices define a column which includes the air parcel (5). Subsequently, within this column, four vertical indices are determined, by locating the indices $(k_{i_{\mathrm{AP}},j_{\mathrm{AP}}}, k_{i_{\mathrm{AP}}+1,j_{\mathrm{AP}}}, k_{i_{\mathrm{AP}},j_{\mathrm{AP}}+1}, k_{i_{\mathrm{AP}}+1,j_{\mathrm{AP}}+1})$ with $\zeta_{k_{i_{\mathrm{AP}},j_{\mathrm{AP}}}} \leq \zeta_{\mathrm{AP}} < \zeta_{k_{i_{\mathrm{AP}},j_{\mathrm{AP}}}+1}$ etc., along the four edges of the column (6). Then, at these four vertical indices and the indices one level higher, the values of ζ_{ijk} and Q_{ijk} are collected to define a box for the interpolation (7). In this box the quantity Q_{ijk} is first interpolated vertically four times to the respective ζ_{AP} (8). Now, the quantity Q_{ijkl} is given on the four corners of the plane with $\zeta = \zeta_{\mathrm{AP}}$ (9). Finally, the quantity is interpolated horizontally, taking into account the line elements of the spherical coordinates (10). This provides $Q(\lambda_{\mathrm{AP}}, \phi_{\mathrm{AP}}, \zeta_{\mathrm{AP}}, t_{\mathrm{AP}})$.

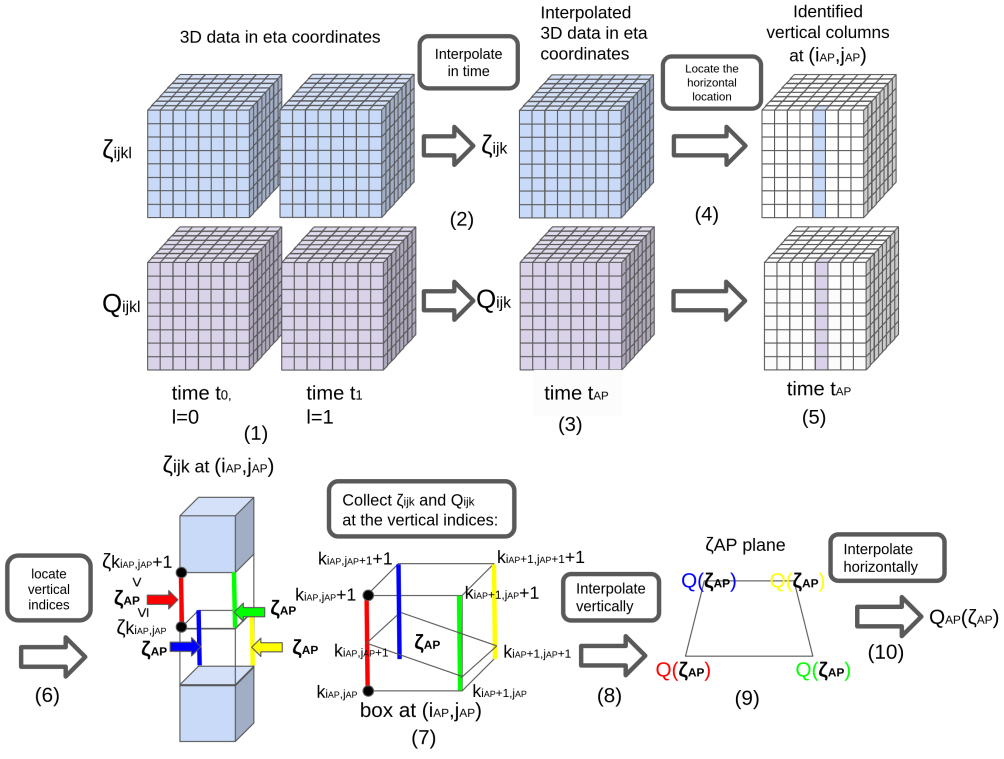

Figure 1. Schematic steps during interpolation V0 of a quantity Q to the air parcel position in zeta coordinates in CLaMS. For further details see the text.

The interpolation from pressure to zeta and from zeta to pressure is particularly important when coupling geophysical modules that operate with pressure as vertical coordinate (e.g. convection, diffusion, and sedimentation), as is the case for MPTRAC. The precise and accurate inversion of the interpolation in CLaMS from pressure back to zeta coordinates is difficult because during step (6) height indices can be found from the pressure that are inconsistent with height indices found using the zeta coordinate positions. If a different box is used for re-interpolation to zeta, significant errors may occur, making this approach unsuitable for frequent transformations between zeta and pressure coordinates. Consequently, a fully reversible

https://doi.org/10.5194/gmd-2023-214
Preprint. Discussion started: 21 November 2023

Geoscientific Model Development Discussions

interpolation algorithm has been developed for MPTRAC to allow the coupling of pressure-based modules with the diabatic advection scheme, where frequent vertical coordinate inversions are required.

Figure 2 shows a schematic of the interpolation in MPTRAC (which we will also refer to as interpolation "V2" in this paper, while it is referred to the original interpolation in MPTRAC as "V1"). With the same definitions as for the interpolation of CLaMS, the interpolation in MPTRAC can be described as follows. The interpolation starts as well by selecting the data of ζ_{ijkl} and Q_{ijkl} for the neighbouring times, i.e. t_0 and t_1 (see Fig. 2 (1)). Then, the horizontal indices of the air parcel are determined $(i_{\mathrm{AP}}, j_{\mathrm{AP}})$ (2). The indices define two columns which include the air parcel at the times t_0 and t_1 (3). Consequently, for each of this columns, four vertical indizes are determined, by locating the indices $(k_{i,j}, k_{i+1,j}, k_{i,j+1}, k_{i+1,j+1})_{t_0}$ and $(k_{i,j}, k_{i+1,j}, k_{i,j+1}, k_{i+1,j+1})_{t_1}$, along the eight edges of the two columns, analogous to the procedure in CLaMS (4). However, afterwards the minimum and maximum index k_{min} and k_{max} among the vertical indices from both times are determined (5). The minimum index and maximum index define the start and end point of an iteration that locates the box that contains the air parcel in vertical direction. The iteration starts with the temporal and horizontal interpolation of ζ_{ijkl} at the bottom and top of a box, which is defined by the minimum vertical index k_{min} and the spatial indices $(i_{\mathrm{AP}}, j_{\mathrm{AP}})$ (see Fig. 2 (6) and (7)). After the interpolation, ζ is given at the top ζ_{top} and the bottom ζ_{bottom} of the box (8). If ζ_{AP} is lower than ζ_{top} and equal or higher than ζ_{bottom}, the iteration finishes. Otherwise, the iteration proceeds by going to the next higher index until the right box is found. Because of the strictly monotonic increase of ζ_{ijkl} with height, it is guaranteed that the right box is found between the minimum and maximum vertical indices. However, when the right box is found, the quantity Q_{ijkl} is interpolated temporally and horizontally as well to the top Q_{top} and Q_{bottom} of the correct box (9), analogous to the interpolation of ζ_{ijkl} in (6) and (7). Finally, the vertical interpolation is performed linearly by using the quantity Q_{ijkl} and the coordinate ζ_{ijkl} from the top and bottom of the box and the zeta coordinate (ζ_{AP}) of the air parcel (9). This provides $Q(\lambda_{\mathrm{AP}}, \phi_{\mathrm{AP}}, \zeta_{\mathrm{AP}}, t_{\mathrm{AP}})$. If Q_{ijkl} is a vertical coordinate, such as pressure, the interpolation can be reversed as the vertical indices in Q_{ijkl} can also be determined in step (4) from the respective vertical Q_{ijkl} profiles.

The algorithm in MPTRAC allows precise interpolation from zeta to pressure and back to zeta, because the vertical column at the horizontal position of the air parcel gives a monotone relationship between zeta and pressure. In particular, the processing of pressure and zeta is analogous with opposite roles. The vertical 1D linear interpolation at the final step (9) can be performed accurately and unambiguously.

https://doi.org/10.5194/gmd-2023-214
Preprint. Discussion started: 21 November 2023

Geoscientific Model Development Discussions

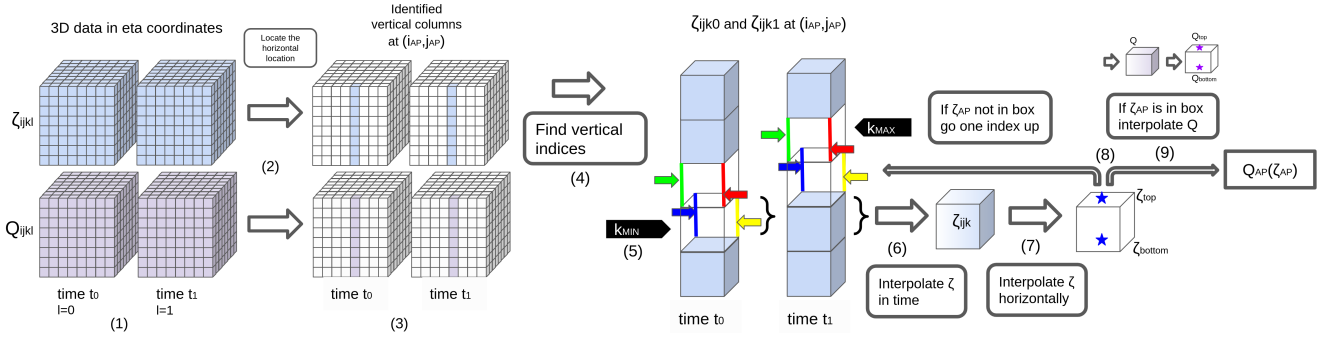

Figure 2. Schematic steps during interpolation V2 of a quantity Q to the air parcel position in zeta coordinates in MPTRAC. For further details see the text.

For the purpose of comparison and error estimations a third interpolation variant was implemented into MPTRAC, that closer resembles the interpolation in CLaMS (called interpolation V3). In this approach the interpolation procedure follows first steps (1) to (3) as defined in V2 and Fig. 2, respectively. Afterwards however, the vertical indices are derived as in CLaMS by averaging the two columns in time before finding the vertical indices and by interpolating on the defined ζ plane (See Fig. 1, steps (4) to (10)).

However, note that all interpolation in MPTRAC are performed in Cartesian coordinates, i.e. the line elements of the spherical coordinate system are not applied during interpolation but afterwards to the final air parcel positions, assuming that the differences of the line elements within a grid box are negligible. The transformation from Cartesian coordinates to spherical coordinates is done separately from the interpolation process, by applying the equations $\Delta\lambda = \frac{\Delta x}{R_e \cos\phi}$ and $\Delta\phi = \frac{\Delta y}{R_e}$. $\Delta x, \Delta y$ denote the changes in Cartesian coordinates, $\Delta\phi, \Delta\lambda$ the change in spherical coordinates and R_e the Earth radius. These transformations are not applied in CLaMS because interpolation already is done in spherical coordinates. Another remaining difference between interpolation in CLaMS and MPTRAC is that the time interpolation is done for each air parcel separately in MPTRAC instead of the full meteorological field as in CLaMS.

2.1.4 Further model differences

MPTRAC uses spherical coordinates to store the position of air parcels. CLaMS has a hybrid approach, with spherical coordinates for air parcels at latitudes between $-72°$ S and $72°$ N, but otherwise uses a stereographic projection at high latitudes (McKenna et al., 2002b). The approach in CLaMS guarantees that the integration does not diverge near the poles.

In MPTRAC the spherical coordinates singularity is handled differently. In MPTRAC, for air parcels very close to the pole (i.e. closer than 110m or $0.001°$ latitude), the zonal transport is ignored. Horizontal coordinates are calculated with double precision to guarantee the required accuracy for this approach. The method has been shown to be reliable for different applications (e.g. Hoffmann et al., 2017; Rößler et al., 2018).

Both models use the shallow atmosphere approximation. This means that the horizontal plane is transformed from spherical to Cartesian coordinates, assuming that the height of the air parcel is negligible with respect to the Earth's radius. The two mod-

https://doi.org/10.5194/gmd-2023-214
Preprint. Discussion started: 21 November 2023

Geoscientific Model Development Discussions

els have slight differences in the Earth's radius. In MPTRAC's default setting, the Earth's radius is assumed to be 6367.421 km, whereas in CLaMS it is 6371.000 km. This has implications for transformations between the Cartesian and spherical coordinate systems.

2.2 Reanalysis data

The full-resolution ERA5, downsampled ERA5, and ERA-Interim reanalyses were used to run the forward trajectory calculations with CLaMS and MPTRAC. ERA5 and ERA-Interim are provided by the ECMWF (Dee et al., 2011; Hersbach et al., 2020). ERA5 is the successor of ERA-Interim. Six-hourly meteorological data at about 80 km horizontal resolution on 60 levels is provided by the ERA-Interim reanalysis. The levels start at the surface, and the upper limit of the reanalysis is at 0.1 hPa. The ERA-Interim reanalysis covers the years from 1979 to 2019. A four-dimensional variational analysis (4D-Var) with a 12 h time window in combination with the ECMWF's Integrated Forecast System (IFS) cycle 31r2 are used for the assimilation of meteorological observations in ERA-Interim.

The ERA5 reanalysis provides hourly meteorological data with 30 km horizontal grid resolution (sampled at $0.3° \times 0.3°$). ERA5 has 137 levels from the surface up to 80 km. In contrast to the ERA-Interim reanalysis, the ERA5 reanalysis was created with the IFS cycle 41r2 and hence benefits from model improvements, such as new parameterisations of atmospheric waves and convection. The assimilation in ERA5 is performed with four-dimensional variational analysis as well. The ERA5 reanalysis provides data for the years between 1950 and the present. It was shown that the ERA5 reanalysis significantly improves Lagrangian transport simulations in the free troposphere and stratosphere and has considerable differences to ERA-Interim (Hoffmann et al., 2019).

The downsampled version of ERA5 (referred to as ERA5 $1° \times 1°$) was computed, applying a truncation to T213 using the ECMWF MARS data processing system. The downsampled version has $1° \times 1°$horizontal sampling and 6 hour temporal sampling. However, ERA5 $1° \times 1°$ has the same vertical resolution as ERA5. ERA5 $1° \times 1°$ is used in transport calculations to profit from enhancements of the ERA5 reanalysis on the one side, but to reduce computing-time and difficulties handling large datasets, such as full-resolution ERA5, on the other side (e.g. Ploeger et al., 2021).

2.3 Diagnostics to evaluate the diabatic transport in MPTRAC

2.3.1 Model runs

For the evaluation of the newly implemented diabatic scheme in MPTRAC, we use a model initialization with about 1.4 million globally distributed trajectory seeds. The forward calculations are calculated for the boreal summer (June, July, August). Short term calculations of 1 day are initialized at the first of July 2016, while the long-term calculations of 90 days are started on the first of June 2016 to cover the entire boreal summer and austral winter. Seasonal differences are taken into account by separately analysing the Northern and Southern Hemisphere. The air parcels are distributed horizontally quasi-homogeneously, so that they have an average mutual distance of about 100 km. Vertically, they are distributed in specific layers. The layers are constructed such that each air parcel represents the same amount of entropy in the atmosphere, which is a product of density

https://doi.org/10.5194/gmd-2023-214
Preprint. Discussion started: 21 November 2023

Geoscientific Model Development Discussions
Open Access
EGU

and the logarithm of the potential temperature (Konopka et al., 2007). For this reason, most air parcels are initialised around the tropopause where the entropy of the atmosphere is largest. However, the air parcels cover a total zeta range from 30 K (about 1 km) to about 2000 K (about 48 km). Setups similar to the one used here are often used to initialise transport calculations with CLaMS for studies in the UTLS, and in particular are constructed to fit the hybrid zeta coordinates and mixing concept in CLaMS (e.g. Konopka et al., 2007; Pommrich et al., 2014; Vogel et al., 2015, 2019; Konopka et al., 2007). In CLaMS air parcels that reach the lower model boundary ($\zeta = 0$) are excluded from any further transport. For the intercomparison with MPTRAC, the same concept was applied in MPTRAC as well.

We employ different simulation scenarios to put the deviations of the two models into the perspective of known uncertainty sources. Table 1 presents the scenarios, where different components of the transport calculations, such as the interpolation, integration, earth radius, coordinate systems, reanalysis, resolution, diffusion parameterisation and the vertical velocity are varied. By comparing these scenarios, we can estimate uncertainties from different sources. Table 2 summarizes the different scenario intercomparisons and the related exposed uncertainty sources.

Table 1. Overview of different simulation scenarios for transport calculations with MPTRAC and CLaMS.

label	reanalysis	model	time-step	integration method	diffusion	inter-polation	Earth radius	vertical velocity	other options
CLaMS-default	ERA5	CLaMS	1800s	Runge-Kutta 4	no	V0	6371000 m	dia.	
CLaMS-def-ERA5 1°×1°	ERA5 1°×1°	CLaMS	1800s	Runge-Kutta 4	no	V0	6371000 m	dia.	
CLaMS-no-pole	ERA5	CLaMS	1800s	Runge-Kutta 4	no	V0	6371000 m	dia.	polar coordinate off
MPTRAC-bestfit	ERA5	MPTRAC	1800s	Runge-Kutta 4	no	V3	6371000 m	dia.	
MPTRAC-bestfit-Re	ERA5	MPTRAC	1800s	Runge-Kutta 4	no	V3	6367421 m	dia.	
MPTRAC-int	ERA5	MPTRAC	1800s	Runge-Kutta 4	no	V2	6367421 m	dia.	
MPTRAC-int-180s	ERA5	MPTRAC	180s	Runge-Kutta 4	no	V2	6367421 m	dia.	
MPTRAC-default	ERA5	MPTRAC	180s	Runge-Kutta	no	V2	6367421 m	dia.	
MPTRAC-def-kin	ERA5	MPTRAC	180s	Runge-Kutta	no	V1	6367421 m	kin.	
MPTRAC-def-diff	ERA5	MPTRAC	180s	Runge-Kutta	yes	V2	6367421 m	dia.	coupled mode
MPTRAC-def-ERA5 1°×1°	ERA5 1°×1°	MPTRAC	180s	mid-point	no	V2	6367421 m	dia.	
MPTRAC-def-erai	ERA-Interim	MPTRAC	180s	mid-point	no	V2	6367421 m	dia.	
MPTRAC-cpl	ERA5	MPTRAC	180s	mid-point	no	V2	6367421 m	dia.	coupled mode
MPTRAC-default-init	ERA5	MPTRAC	180s	mid-point	no	V2	6367421 m	dia.	initial ζ minus 0.1 K

https://doi.org/10.5194/gmd-2023-214
Preprint. Discussion started: 21 November 2023

Geoscientific Model Development Discussions
Open Access
EGU

Table 2. Scenario intercomparisons for the estimation of different uncertainties in the Lagrangian transport calculations. Two scenarios are compared (base and comparative scenario) for the estimation. In most cases only one aspect of the model set-up is varied. The first block focuses on internal uncertainties of CLaMS and MPTRAC separately. The second block focuses on the external uncertainties. The third block focuses on the comparison of the two models. The last block show miscellaneous set-ups. The difference of the start to the end point of a trajectory for an air parcel is not an uncertainty source (in Tab. 2 referred to as "transport"), but it is useful quantity to compare with the magnitude of inferred uncertainty sources.

uncertainty source	Scenario basis	comparative scenario	Difference
p-zeta-p transformation	MPTRAC-default	MPTRAC-cpl	coupled vs. uncoupled mode
Integration scheme	MPTRAC-default	MPTRAC-int-180s	Only vary integration scheme
Time-step	MPTRAC-int	MPTRAC-int-180s	Only vary between 1800s and 180s time steps
Interpolation	MPTRAC-bestfit	MPTRAC-int	Only vary interpolation method
Polar coordinates	CLaMS-default	CLaMS-nopoles	Only vary polar coordinate switch
Earth radius	MPTRAC-bestfit	MPTRAC-bestfit-Re	Only vary used Earth radius
Combined internal	MPTRAC-default	MPTRAC-bestfit-Re	Combined internal uncertainty of MPTRAC
Diffusion	MPTRAC-default	MPTRAC-def-diff	Only vary usage of diffusion and sub-grid scale wind module
Downsampling	MPTRAC-default	MPTRAC-def-ERA5 1°×1°	Only vary ERA5 to ERA5 1°×1°
Reanalysis	MPTRAC-default	MPTRAC-def-erai	Only vary ERA5 to ERA-Interim
Vertical velocity	MPTRAC-default	MPTRAC-def-kin	Vary vertical velocity
Model default	MPTRAC-default	CLaMS-default	Compare default setup of models
Model default 1°×1°	MPTRAC-def-1°×1°	CLaMS-def-1°×1°	Compare default setup of models at lower resolution
Model best fit	MPTRAC-bestfit	CLaMS-nopoles	Compare closest setup of models
Initial bias	MPTRAC-default	MPTRAC-default-init	Default shift initial positions with -0.1 K
Transport	MPTRAC-default	MPTRAC-default	Compare end position with start positions

The sources of uncertainty are classified into internal, model and external uncertainties. Internal sources for model uncertainties are based on the model code of a Lagrangian transport model itself, such as variation in the interpolation scheme or coordinate system. These uncertainties are not estimated by comparing two different models but by comparing two different set-ups of the same model and hence give an indication of the order of magnitude of the uncertainty already present within a model. A combination of all internal uncertainty sources within MPTRAC (interpolation, integration scheme, earth radius and time-step) is as well investigated (combined internal uncertainty).

Model uncertainties are the combination of uncertainties between two models. Often, the sources that cause the model uncertainties are not known. The model uncertainties can be caused by the estimated internal uncertainties if the models also differ in the methods used. However, additional sources of uncertainties are possible. For example, the interpolation methods between MPTRAC and CLaMS vary more than can be estimated from the variation in the interpolation methods implemented in MPTRAC. While the interpolation in MPTRAC is always in Cartesian coordinates, CLaMS uses spherical coordinates.

External uncertainty sources are those given as limitations of ECMWFs weather forecasting models providing ERA5 and ERA-Interim reanalysis data. The physical accuracy of the reanalysis model as well as its resolution play a role in the un-

https://doi.org/10.5194/gmd-2023-214
Preprint. Discussion started: 21 November 2023

Geoscientific Model Development Discussions

certainty. Therefore, different reanalysis products such as ERA5, ERA-Interim and ERA5 $1^\circ \times 1^\circ$ lead to different trace gas transport in MPTRAC and CLaMS. In addition, diabatic and kinematic velocities in the reanalyses are generally also inconsistent. Note that the magnitude of calculated uncertainties can depend from an other source of uncertainty. For example the interpolation error increases when the reanalysis data is downsampled or the integration errors are reduced when singularities at the poles are avoided with a more suitable coordinate system.

Moreover, we compared a scenario with a bias of -0.1 K to the initial air parcel positions and the default scenario of MPTRAC (Initial bias). We as well compared the initial positions and the final position of the air parcels as a measure of magnitude for the actual transport process.

2.3.2 Diagnostics for model uncertainties and differences

For the intercomparison of the different model scenarios, we apply a set of frequently used diagnostics (e.g. Stohl et al., 1995; Hoffmann et al., 2019). Let i and j denote the indices of two trajectories, and t the time at which the comparison is done. Then the air-parcel-wise absolute vertical transport deviation (AVTD) at a given time t in the vertical zeta coordinate is

$$\mathrm{AVTD}_\zeta = |\zeta_i(t) - \zeta_j(t)|. \tag{6}$$

The absolute deviation in vertical direction quantifies the differences between individual air parcels.

The log-pressure altitude is defined as $Z = H \log \frac{p0}{p}$, where $p_0 = 1013.25$ and $H = 7.0$. Then, the air-parcel-wise absolute vertical transport deviation (AVTD) in log-pressure altitude is:

$$\mathrm{AVTD}_Z = |Z_i(t) - Z_j(t)|. \tag{7}$$

To calculate the air-parcel-wise absolute horizontal transport deviation (AHTD) we use

$$\mathrm{AHTD} = \sqrt{(x_i(t) - x_j(t))^2 + (y_i(t) - y_j(t))^2}, \tag{8}$$

where (x_i, y_i) and (x_j, y_j) are the positions of the air parcels in Cartesian coordinates.

To measure the conservation error of a quantity q such as potential temperature at time t, the air-parcel-wise relative tracer conservation error (RTCE) is used,

$$\mathrm{RTCE} = 2 \frac{|\, q(t) - q(0) \,|}{|\, q(t) \,| + |\, q(0) \,|}. \tag{9}$$

Individual trajectories of air parcels can substantially deviate between the scenarios defined in Table 1. Statistics such as quantiles, means, and medians of the different air-parcel-wise diagnostics for about 1.4 Mio. air parcels are considered to robustly quantify deviations independent of single air parcel outcomes. Note that Stohl et al. (1995); Hoffmann et al. (2019) define the absolute trajectory deviations and conservation errors as the average over the above air-parcel-wise absolute trajectory deviations. Here we in contrast refer to the air-parcel-wise diagnostic with AVTD, AHTD and RTCE, and mention the statistical moments and quantiles explicitly (e.g. mean AVTD for the average over all air-parcel-wise AVTDs).

https://doi.org/10.5194/gmd-2023-214
Preprint. Discussion started: 21 November 2023

Geoscientific Model Development Discussions

3 Results

3.1 Examples of trajectories and transport deviations

The simulations are initialized globally and cover almost the entire height range of the free troposphere and stratosphere (about 1-50 km), allowing for the analysis of numerous meteorological conditions and different trajectories. Figure 3 shows exemplary trajectories for a duration of 10 days, highlighting transport in the troposphere, quasi-horizontal transport in the upper troposphere and lower stratosphere (UTLS), and fast transport in the lower stratosphere (LS).

These examples show that the differences among the models are significantly smaller than the external differences associated with the downsampling of reanalysis data, different vertical velocities, variations in reanalysis datasets (here from ERA5 to ERA-Interim), or the impact of atmospheric diffusion. Trajectories with ERA5 $1° \times 1°$ roughly follow the fully resolved ERA5 calculations, although deviations still need to be taken into account. However, when particle diffusion resulting from sub-grid scale winds and turbulence is parameterized, the trajectories have significant variations compared to the unparameterized trajectories. Particularly in the stratosphere, the altitude shows pronounced variability relative to the low average vertical transport during this time period. The statistical significance of these findings will be discussed in the subsequent chapters, which will contain the entire ensemble of 1-day forward trajectories and is later extended to 90 days calculations as well.

https://doi.org/10.5194/gmd-2023-214
Preprint. Discussion started: 21 November 2023

Geoscientific Model Development Discussions

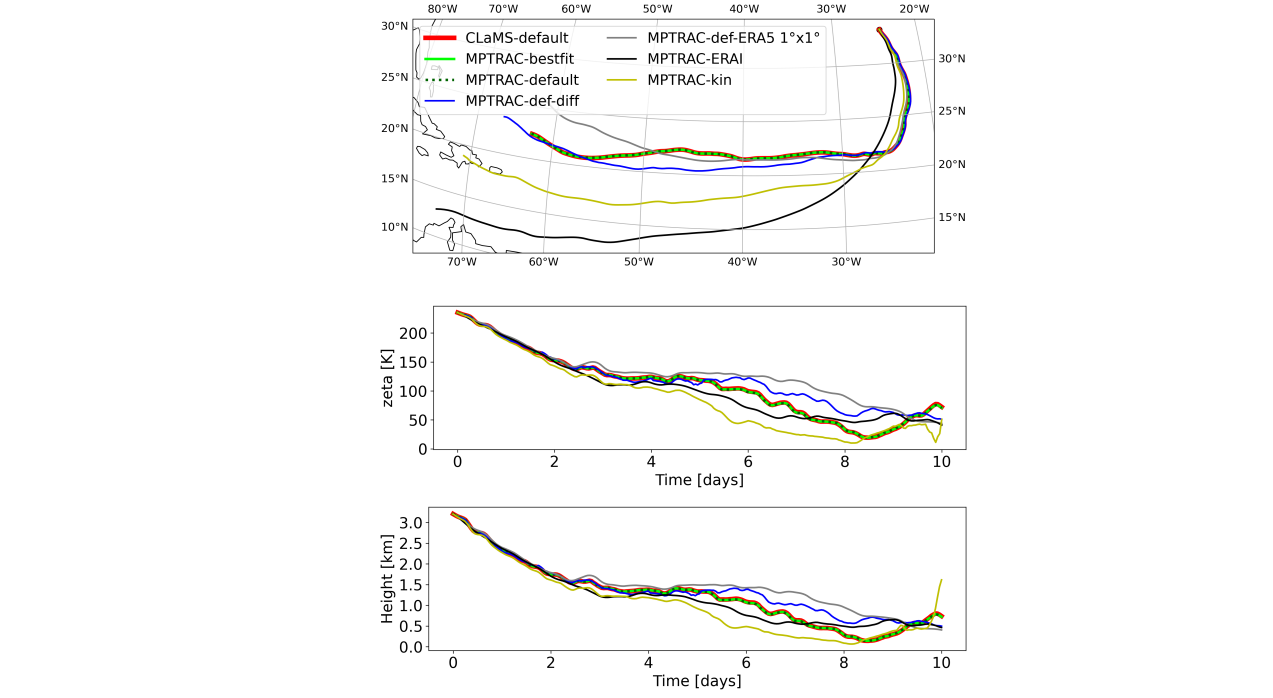

(a)

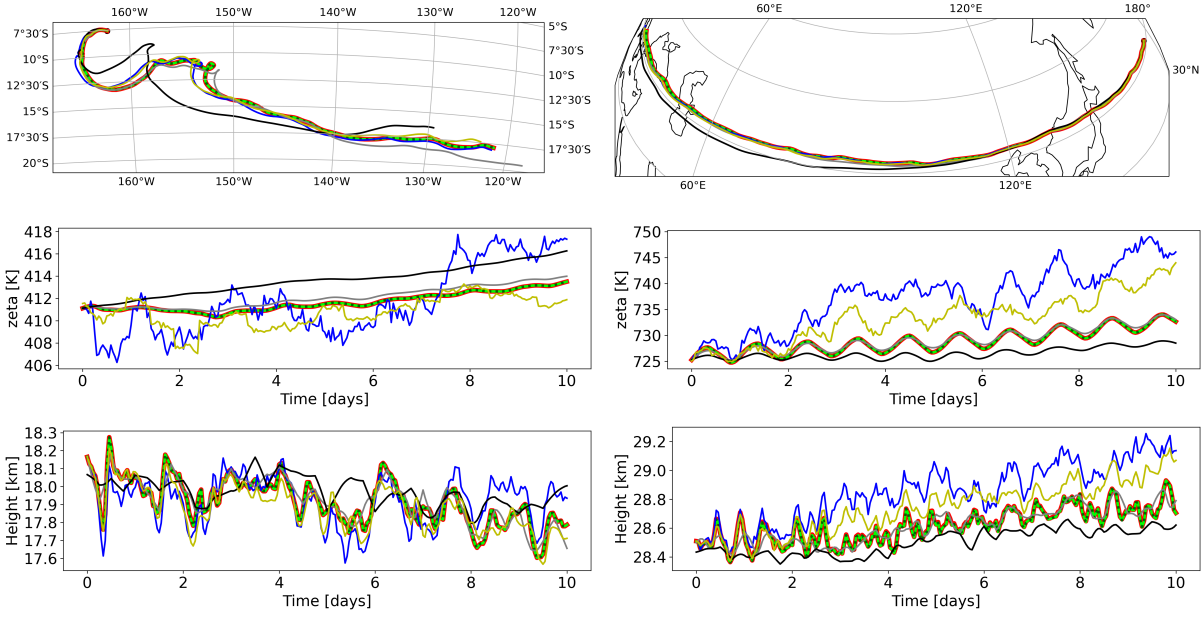

(b) (c)

Figure 3. Selection of trajectories calculated 10 days forward from 1 July 2016. Calculation results for different scenarios for three examples are shown: (a) Example for the troposphere, (b) example for the UTLS and (c) example for the lower stratosphere. For each trajectory the horizontal transport is shown in theupper panel. The vertical transport in the zeta coordinates and in log-pressure height is depicted below.

https://doi.org/10.5194/gmd-2023-214
Preprint. Discussion started: 21 November 2023

Geoscientific Model Development Discussions

3.2 Transport uncertainties over 1 day

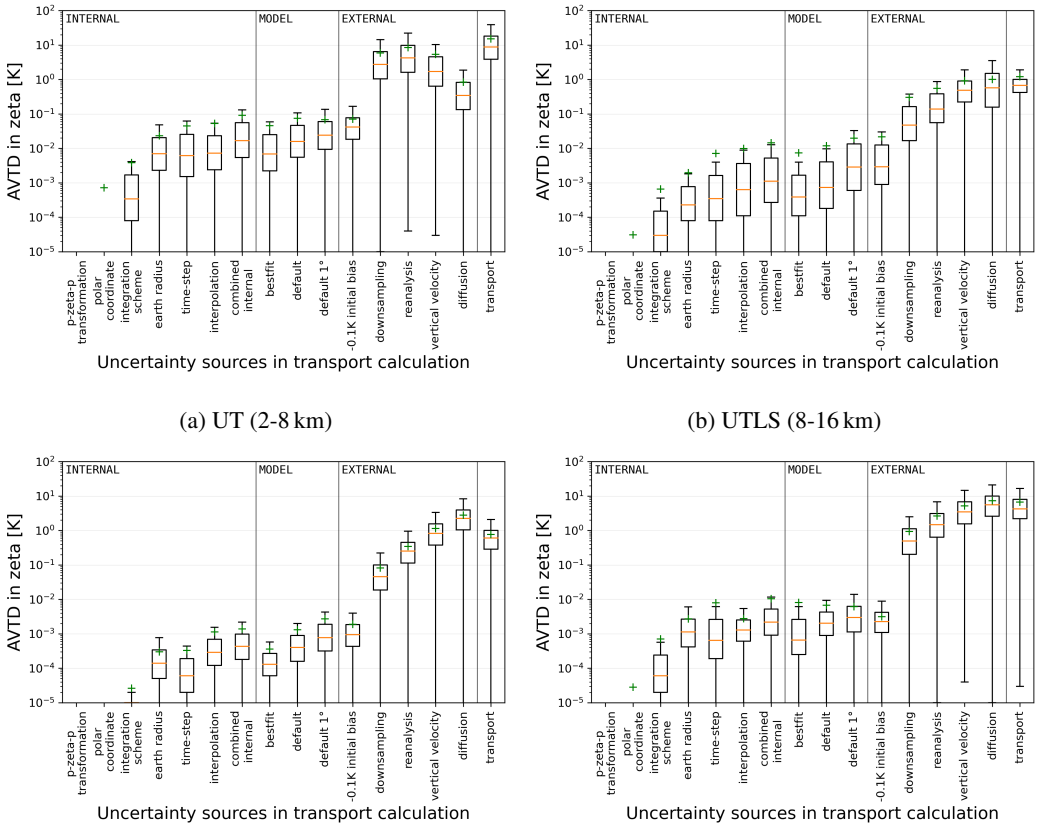

(a) UT (2-8 km)

(b) UTLS (8-16 km)

(c) LS (16-32 km)

(d) US (32-48 km)

Figure 4. Different AVTDs in zeta coordinates after 1 day forward calculations for the entire ensemble of air parcels splitted into four height layers. The box plots show the median, quartiles (25% and 75%), minimum and maximum (outliers have been ignored if they are 1.5 times the inter-quartile difference). Green crosses indicate the mean AVTDs. Deviations for the p-zeta-p transformation and the polar coordinate are lower than 10^{-5} K and do not show up here. The distinction between internal, model and external uncertainty sources is indicated by vertical lines.

https://doi.org/10.5194/gmd-2023-214
Preprint. Discussion started: 21 November 2023

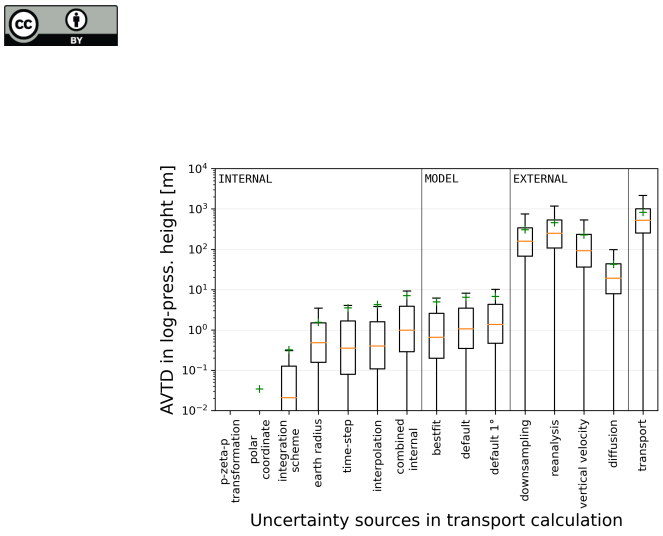

(a) UT (2-8 km)

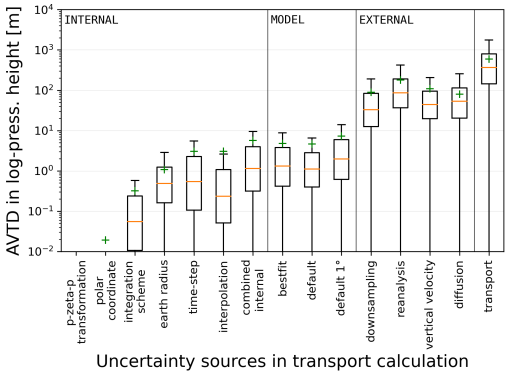

(b) UTLS (8-16 km)

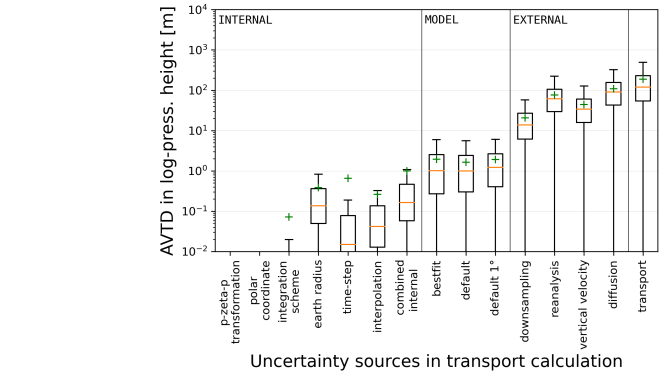

(c) LS (16-32 km)

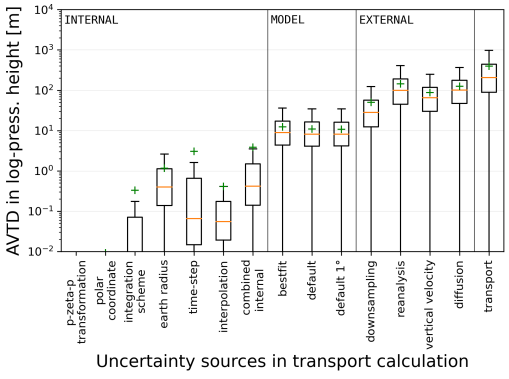

(d) US (32-48 km)

Figure 5. AVTDs in log-pressure heights after 1 day forward calculations for the entire ensemble of air parcels splitted in four height layers. The boxplots indicate quartiles as defined in Fig. 4.

https://doi.org/10.5194/gmd-2023-214
Preprint. Discussion started: 21 November 2023

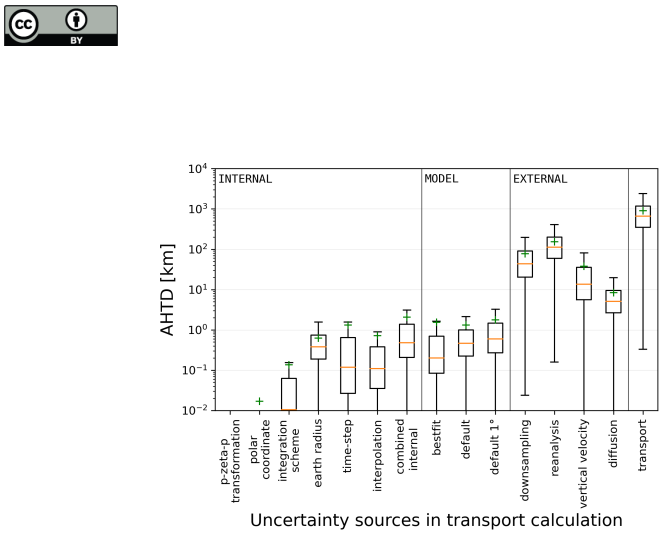

(a) UT (2-8 km)

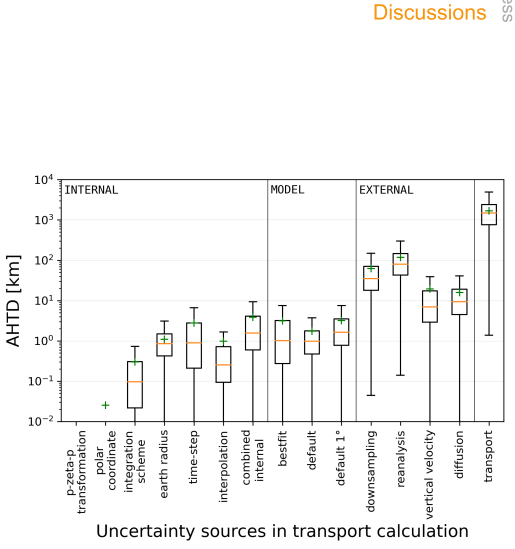

(b) UTLS (6-16 km)

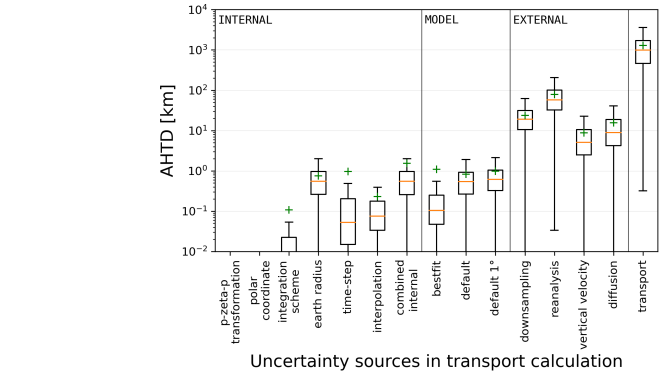

(c) LS (16-32 km)

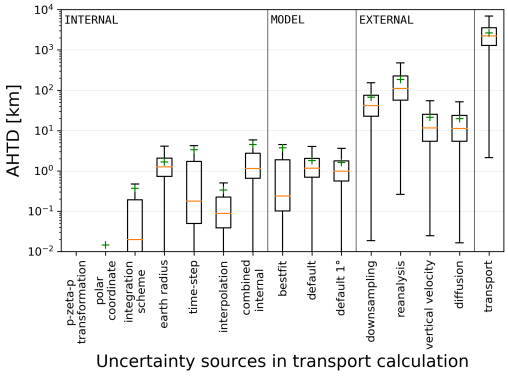

(d) US (32-48 km)

Figure 6. AHTDs after 1 day forward calculation for the entire ensemble of air parcels splitted in four height layers. The boxplots indicate quartiles as defined in Fig. 4.

Figure 4 presents statistics for vertical transport deviations after one day of calculations in the hybrid zeta coordinates. Different height ranges are displayed depending on the initial position of the air parcels. Throughout the troposphere and stratosphere, model differences measured by the AVTD in the zeta coordinate are on the order of magnitude of the combined known internal uncertainties within individual models (10^{-4} K to 10^{-2} K). This is valid for the scenarios with the full ERA5 and ERA5 $1° \times 1°$, although uncertainties increase in the latter scenario (see Fig. 4 at the labels "default" and "default 1°").

Separately assessed, the variation of the Earth radius, the time step variation from 180 s to 1800 s in the Runge-Kutta method and the interpolation variation in MPTRAC are estimated to cause transport uncertainties lower than 10^{-1} K between 2-8 km and lower than 10^{-2} K at higher levels (see Fig. 4 at the labels earth radius, time-step and interpolation). Since the choice of the time-step between 1800 s and 180 s shows considerable internal differences, time-steps of 180s as applied in MPTRAC are advised. Moreover, with a time-step of 180 s the variation of the integration schemes from the mid-point scheme to the Runge-Kutta scheme shows minor transport differences (see Fig. 5 at the label "integration scheme").

https://doi.org/10.5194/gmd-2023-214
Preprint. Discussion started: 21 November 2023


Geoscientific Model Development Discussions

Only limited to trajectories in proximity to the poles, uncertainties due to the coordinate singularity must be considered. However, the transformation from spherical coordinates to the stereographic projection at high latitudes causes deviations similar to deviations related to the selection of the integration method. Larger deviations that are restricted to the pole, increase the mean AVTD in Fig. 4 over 10^{-5} K. The p-zeta-p transformation within MPTRAC, which combines pressure-based modules with zeta-based advection, is shown to cause transport uncertainties that are orders of magnitude smaller than the other uncertainty sources. These two uncertainty sources related to coordinate transformations are the internal uncertainties of the least importance (see Fig. 5 at the labels "p-zeta-p transformation", "polar coordinate").

Model differences are one to three orders of magnitude smaller than uncertainties resulting from external factors ($\sim 10^{-1} - 10$ K) in the hybrid zeta coordinate (see Fig. 4). Diffusion from parameterised sub-grid scale winds and turbulence leads to median AVTDs up to about 10 K after 24 hours, which is close to the overall transport median which is a measure of the distance air parcels take (median AVTD between the initial positions and the end points). Diffusion is the largest uncertainty at all layers, except between 2-8 km, where the reanalysis uncertainty is the largest source of uncertainty. The second largest uncertainty in zeta coordinates is given by the variation of the vertical velocity ($\sim 1\,\text{K} - 10\,\text{K}$). Reanalysis variations, such as between ERA-Interim and ERA5, exhibit median AVTDs of approximately 0.5 K. ERA5 $1^\circ \times 1^\circ$ shows a deviation of 0.1 K compared to the full-resolution ERA5. Moreover, the identified model differences are of the same order as a propagated initialization bias of -0.1 K. The bias of 0.1 K increases by approximately 0.01 K after 24 hours through error propagation. Hence, uncertainties after 1 day are likely influenced equally by model uncertainties and uncertainties of the initial data.

Finally, when the CLaMS and MPTRAC models are configured to operate in the most similar manner, the model uncertainty is substantially reduced. Some remaining uncertainties are expected related to small remaining differences in the interpolation scheme or from differences in the compilation flags.

Figure 5 shows the same statistics as Fig. 4 but for log-pressure coordinates. For the height range between 2 km and 32 km the median AVTD in log-pressure coordinates between the two models in default set-up is $\sim$ 1 m. At higher levels (32-48 km) the median AVTD is 10 m. While the median AVTD between the models is around the same order of magnitude as the combined internal uncertainty between 2 km and 16 km as found in the hybrid zeta coordinates, in log-pressure coordinates the deviations are up to two order of magnitudes larger than the combined internal uncertainty. This is a consequence of the transition from linear to logarithmic interpolation of pressure in CLaMS at higher altitudes starting from 500 K. Moreover, in the stratosphere, the median AVTD between initial and final positions after 1 day is larger than the deviation from vertical diffusion in the pressure coordinate, in contrast to the median AVTD in zeta coordinates, because the transport in the UTLS is mostly isentropic and hence might cross multiple isobars but less isentropes (see Fig. 4 and 5 at the labels "diffusion" and "transport" for the layers UT and LS).

When the AHTDs are considered, qualitatively very similar results to the vertical transport deviations are obtained. The horizontal model differences and internal uncertainties are of the order of 0.1 km to 10 km after one day of calculations, while external uncertainties lead to absolute horizontal deviations of the order of 10 km to 100 km (see Fig. 6). The difference between initial and final positions is around 1000 km. For the horizontal deviations variations of reanalysis and the downsampling

https://doi.org/10.5194/gmd-2023-214
Preprint. Discussion started: 21 November 2023

become more important than uncertainty sources such as the vertical velocity, because the later does not alter horizontal velocities directly, while the first immediately alter the horizontal transport velocities.

From an overall statistical perspective, as depicted by the Figs. 4 to 6, different layers show different uncertainties. To emphasize the vertical and hemispheric (i.e. seasonal) dependencies of transport uncertainties, Fig. 7a shows the hemisphere-wise vertical mean profiles for a selection of uncertainty sources. Please note the logarithmic scale and that the average AVTD differs from the median AVTD because of the skew distribution of trajectory deviations. First, it is evident again, that all uncertainties from external sources are orders of magnitudes larger than uncertainties from internal sources and deviations between the models. Second, all uncertainties, except those due to parameterized diffusion, exhibit the largest absolute mean deviations in the troposphere (below 330K). The smallest mean AVTD in the zeta coordinate can be found between 330 K and 750 K in the LS, while the deviations above 750 K increase again with height. In comparison to absolute deviations, relative deviations (see Fig. 7b) show less dependency on height (The relative deviations are normalized to the sum of all incremental 1 hour transport steps calculated with the default set-up of CLaMS). While the troposphere has highest relative uncertainties, the stratosphere shows lower relative uncertainties, which are also mostly independent of height. This indicates that the increase of the mean AVTD in the stratosphere is a consequence of larger zeta gradients with height. Zeta levels are closer together in the upper stratosphere, so that air parcels cross more levels at those heights during the transport process.

The profiles of the transport uncertainties are similar in the two hemispheres. However, if hemispheres are compared in more detail, the strongest relative internal uncertainties are found in the winter hemisphere. Absolute and relative uncertainties in the Northern Hemisphere, specifically in winter, are most likely much larger in the stratosphere due to the influence of the polar vortex and increased wave activity in winter. This seasonality was found by Hoffmann et al. (2019) with kinematic transport calculations as well. In particular, the integration time-step becomes the dominant internal uncertainty sources in the region of the polar vortex, because high zonal velocities require short time-steps for stable integration, which is not always fulfilled with 1800 s time-steps for the ERA5 reanalysis (see also Appendix A). This shows that increasing resolution of the reanalyses can only be exploited completely with models that efficiently run at short time-steps.

Moreover, the vertical profiles in Fig. 7 reveal that throughout the atmosphere the deviation from variation of the vertical velocity is larger than the deviation from the variation of the reanalysis, which in turn is larger than the change from ERA5 to ERA5 $1^\circ \times 1^\circ$. In particular uncertainties from diffusion are lowest up to the middle troposphere, increases sharply up to around the tropopause, where it becomes the largest source of uncertainties. Afterwards the uncertainty from diffusion decreases slowly at higher levels again back to uncertainty ranges comparable to the uncertainty from variation of reanalysis. The results show that the implementation of diabatic vertical transport into MPTRAC has a significant impact, comparable to other external uncertainties.

https://doi.org/10.5194/gmd-2023-214
Preprint. Discussion started: 21 November 2023

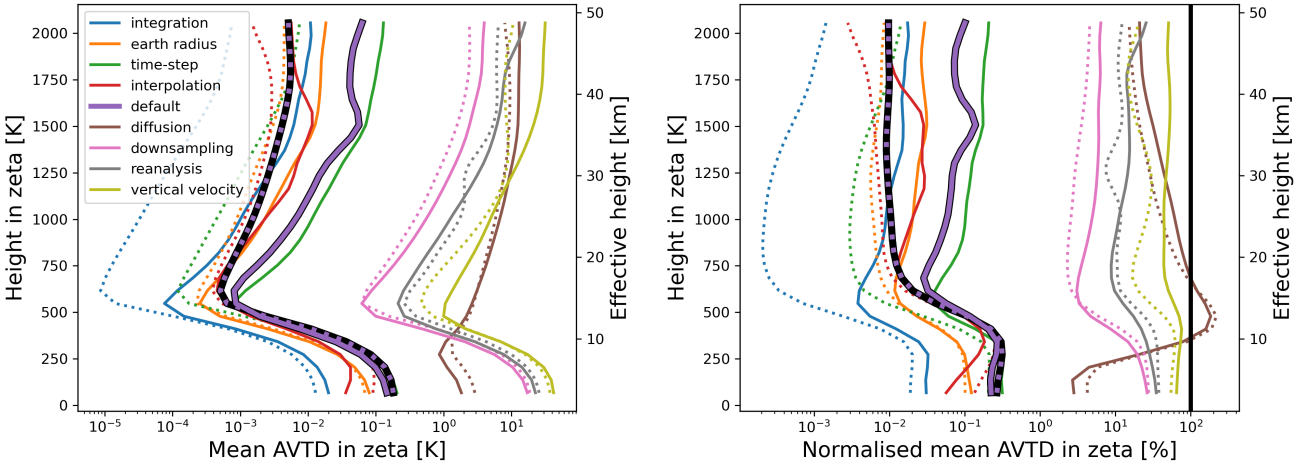

(a) Absolute

(b) Relative

Figure 7. Smoothed vertical profiles of hemispheric average AVTD in zeta coordinates. (a) absolute values and (b) relative values, where the deviations are normalised to the mean vertical path-length calculated with the default set-up of CLaMS (see "CLaMS-default" in Table 1). The dotted lines indicate uncertainties of the Southern Hemisphere (austral winter), and solid lines indicate uncertainties of the Northern Hemisphere (boreal summer). The effective height is the average log-pressure height at a zeta level at the beginning of the calculations. The black vertical line in panel (b) marks 100%.

3.3 Uncertainty growth during 90 day forward calculations

To investigate the uncertainty growth between the CLaMS and MPTRAC models and to better understand the model differences in the context of other uncertainties, trajectory calculations were performed for 90 days starting from 1 June 2016. Figure 8 displays the temporal evolution of the transport deviations between the two models (labeled "default"), along with the downsampling, vertical velocity, reanalysis and diffusion transport uncertainties. For the intercomparison of the two models we use the default configuration of the models (see "Model default" in Table 2) as they represent the usual uncertainty that has to be expected.

The agreement between the models and transport uncertainties varies significantly with height. In the upper troposphere, vertical transport uncertainties remain below 1 K only for a short period (a few hours to days) due to the strong mixing and convection. Subsequently, uncertainties in this region grow rapidly with up to 4.3 K per day. In particular, the selection of the reanalysis and downsampling cause fast divergence in the troposphere. The median model difference is smaller than uncertainties related to changes in reanalysis data, downsampling of the data, or parameterised sub-grid scale winds and diffusion. The median difference between the two models remains below approximately 1 K for the first week. Subsequently, there is also a sharp increase (up to 2.2 K per day), reaching a median difference of about 55 K at 40 days of simulation time, where the different uncertainties reach a similar magnitude.

https://doi.org/10.5194/gmd-2023-214
Preprint. Discussion started: 21 November 2023

In the lower and upper stratosphere, the vertical transport deviations remain lower because air parcels mainly move isentropic. Additionally, horizontal mixing is much less in most regions of the lower and upper stratosphere in contrast to the troposphere. The median model deviation is again much smaller than all other uncertainty sources, but now for the entire 90-day integration period. In the lower stratosphere, 50% of the air parcels have an model difference lower than 1 K for approximately two months and afterwards the deviation still increases slowly (not more than 0.16 K per day). In the upper stratosphere, the same criterion is met after around 34 days, also with a slow to moderate increase afterwards (not more than 1.2 K per day).

Uncertainties from the selection of the vertical velocity and the reanalysis are of similar importance. In the UTLS and at higher altitudes, the variation of the vertical velocity first shows slightly larger uncertainties than the variation of the reanalysis. However, after a couple of weeks, the uncertainty from reanalysis selection is higher, because the choice of the vertical velocity does not affect the horizontal wind speeds as it is the case for the choice of the reanalysis. The smallest transport uncertainty from external sources throughout the atmosphere is given by the ERA5 $1° \times 1°$ data, because ERA5 $1° \times 1°$ has the same vertical resolution and similar horizontal velocities as the ERA5 reanalysis. Finally, in the UTLS results lie in between the pure stratosphere and the upper troposphere, influenced by the transport of air parcels between the stratosphere and troposphere.

The differences between the two models have an impact on the horizontal distribution of the air parcels as well (Fig. 9). While the models median AHTD is less than 1000 km for 40 to 60 days in the stratosphere, it is less than 1000 km only for 15 to 20 days in the UT and UTLS. In the UTLS and UT air parcels deviations reach an upper boundary, where further uncertainty growth stagnates for all scenarios, after around 40 days. In the stratosphere this boundary is approached after 60 to 90 days for external uncertainty sources, while it is not completely approached by the model difference in this time period. Moreover, the horizontal deviations for the scenario with ERA5 $1° \times 1°$ grow considerable as well throughout the atmosphere, indicating that air parcels are often not in good agreement with the full-resolution ERA5 reanalysis.

https://doi.org/10.5194/gmd-2023-214
Preprint. Discussion started: 21 November 2023

Geoscientific Model Development Discussions

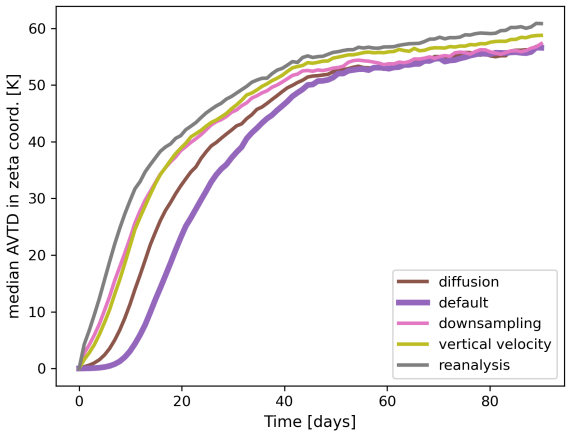

(a) UT (2-8 km)

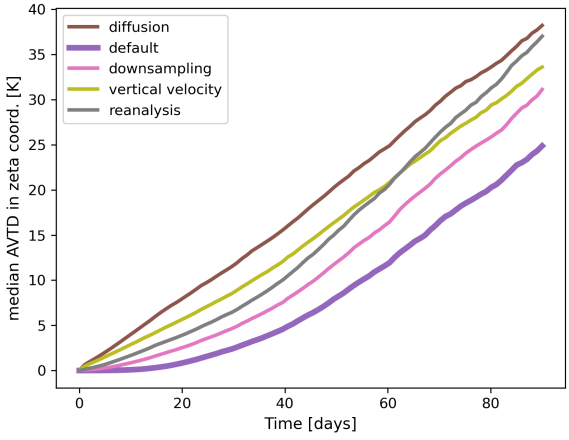

(b) UTLS (8-16 km)

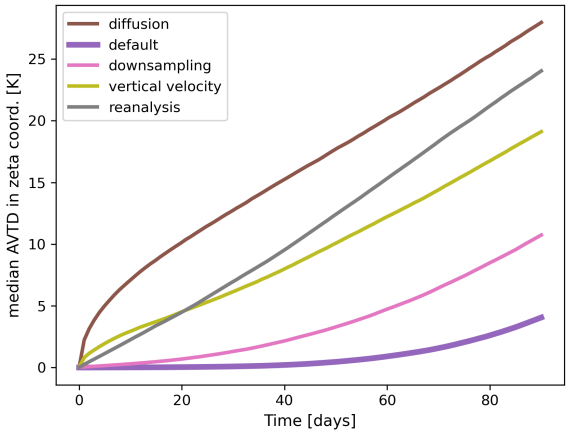

(c) LS (16-32 km)

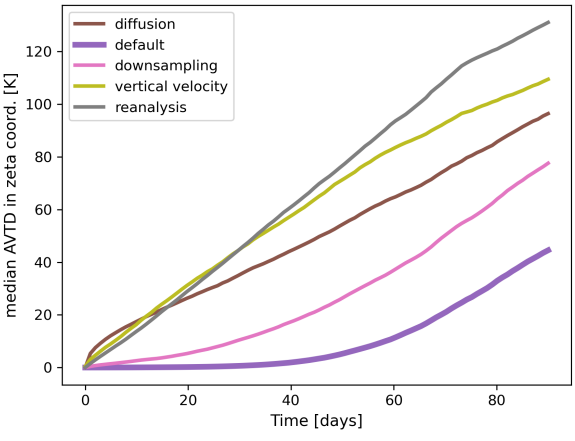

(d) US (32-48 km)

Figure 8. Evolution of the median AVTD in the zeta coordinate for different uncertainty sources for 90 days. The median AVTD between the two models is labeled "default" as defined in Table 1. The starting date is the 1 June 2016. The classification into the layers is done with the initial heights of the air parcels.

https://doi.org/10.5194/gmd-2023-214
Preprint. Discussion started: 21 November 2023

Geoscientific Model Development Discussions

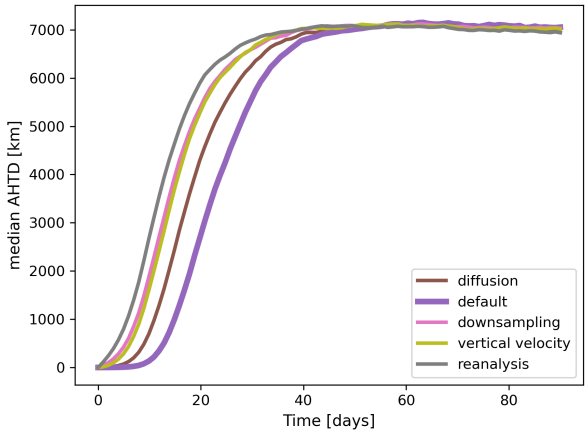

(a) UT (2-8 km)

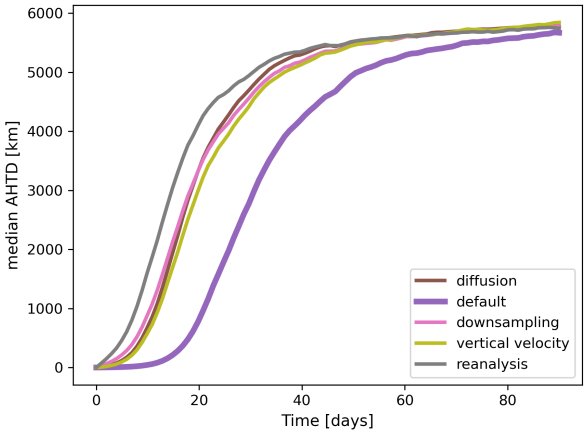

(b) UTLS (6-16 km)

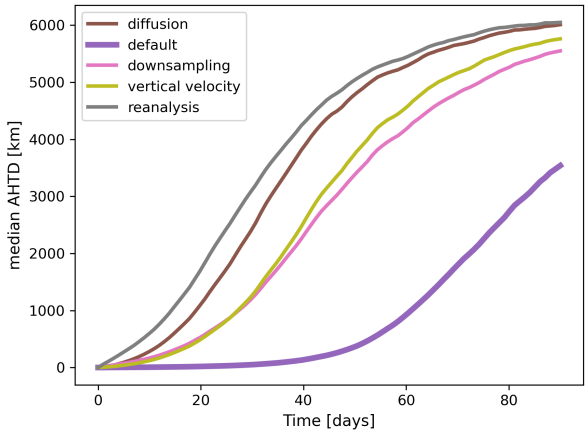

(c) LS (16-32 km)

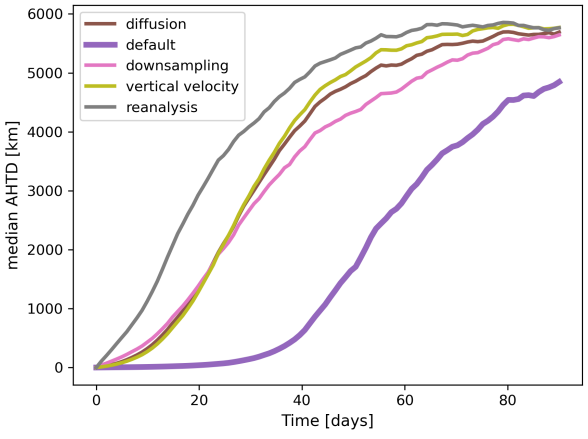

(d) US (32-48 km)

Figure 9. Evolution of the median AHTD of different uncertainty sources for 90 days. The median AHTD between the two models is labeled "default" as defined in Table 1. The starting date is the 1 June 2016. The classification into the layers is done with the initial heights of the air parcels.

3.4 Air parcel distribution on seasonal timescales

Since individual trajectories are not expected to agree over time periods of several months, the statistical distribution of air parcels after 90 days integration period is used to quantify the differences between the models and the uncertainty related to external sources. For reference, the initial density of the air parcels is shown in Fig. 10a. Figure 10b shows the zonal mean distribution of air parcels after 90 days of forward calculations for the CLaMS model with its default setup. After 90 days, the density is highest around the vertical level of 450 K, where most of the air parcels have been transported to within the shallow

https://doi.org/10.5194/gmd-2023-214
Preprint. Discussion started: 21 November 2023

Geoscientific Model Development Discussions
Open Access
EGU

and deep branch of the Brewer-Dobson circulation (BDC). Air parcels also accumulate below the tropopause and near the surface below 2 km (where the models are configured to terminate the air parcel trajectories). This is a consequence of up- and downdrafts in the troposphere combined with the tropopause as an upper transport barrier and the ground as the lower transport barrier.

Furthermore, more air parcels are leaving the Northern Hemisphere than entering it in our calculations, i.e. the cross-equatorial flow in the UTLS increases the air parcel density in the Southern Hemisphere relatively to the Northern Hemisphere. As indicated by averaged trajectories in Fig. 10b the hemispheric asymmetric distribution of air parcels is mostly related to the strength of the southern hemispheric, shallow branch of the BDC, that is located between 40° S and 5° N in latitude and crosses the equator, respectively.

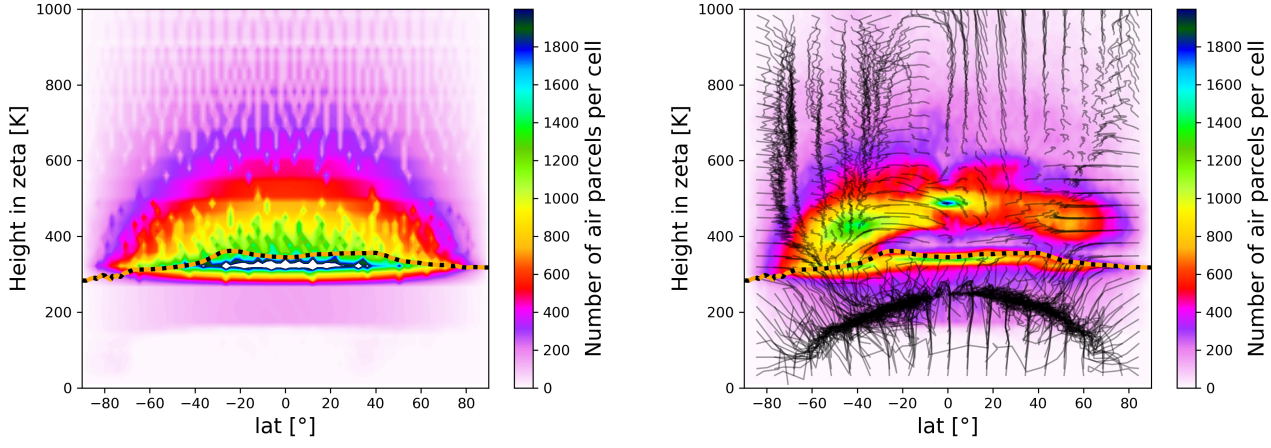

(a) Initial Condition

(b) CLaMS default, final positions

Figure 10. Initial and final air parcel distribution after 90 days when calculated with the CLaMS default set-up. Black lines show box-wise averaged trajectories to indicate the average circulation of the trajectories. The orange dotted line indicates the 90 days average tropopause.

The transport found in the MPTRAC results is almost identical to the CLaMS model as can be seen in Fig. 11a, where the bias between the air parcel distributions of both models is shown as well as contour lines of air parcel frequencies after 90 days forward calculations. The contour lines of the air parcel frequencies align very well around the tropopause and at higher levels at around 500K. Overall, there is no significant bias found between the air parcel distribution of the two models. Except for statistical noise, the simulation results of CLaMS and MPTRAC are in excellent agreement. This is in distinct contrast to biases found for other known uncertainties, as will be discussed below.

When the diffusion module (see Fig. 11b) is switched on in MPTRAC, the patterns without diffusion are reproduced as well, but with smoothed peaks (in Fig. 11b green contours shrink in comparison to black contours). Less air parcels are found in the height region where the frequency of air parcels peaks for the default scenarios of MPTRAC and CLaMS (around 450 K, see also Fig. 11f), whereas the frequencies are increased at the neighbouring levels. The result indicate, that the mean

https://doi.org/10.5194/gmd-2023-214
Preprint. Discussion started: 21 November 2023

Geoscientific Model Development Discussions

distribution is not affected by the sub-grid scale diffusion, except for a smoothing effect. It can be shown that diffusion causes large cross-isentropic dispersion (see Appendix Fig. C1).

The downsampling of the ERA5 data (see Fig. 11c) has only minor impact on the distribution of air parcels above the tropopause. The largest differences can be found at the tropical tropopause and in the troposphere. With ERA5 $1° \times 1°$, more air parcels remain located within the troposphere after 90 days. This is likely a consequence of reduced vertical transport in convective events in the ERA5 $1° \times 1°$ in comparison to the full resolution data, which is in agreement with other studies (e.g. Hoffmann et al., 2023b). With weaker vertical transport, more air parcels remain in the troposphere and less air parcels are transported downward into the model boundary layer, where they are terminated.

With ERA-Interim, qualitatively very different result are found (see Fig. 11d). The BDC transport in the tropics is faster with ERA-Interim than with ERA5 between levels around 400 K to 600 K. Hence, more air parcels are transported from around 400 K to around 600 K in ERA-Interim. At the same time, the transport at higher levels than 600 K is slower with ERA-Interim than with ERA5, which decreases the air parcel number relative to ERA5 above 700 K. The upward transport in the upper part of the shallow branch is faster in ERA-Interim than in ERA5 as well. Hence more air parcels are found at higher altitudes around latitudes of 45° S with ERA-Interim (see also Appendix B1d). This results are in agreement with climatological findings (e.g. Ploeger et al., 2021). Additionally, more air parcels are found between the 400 K level and the tropopause with ERA-Interim than with ERA5 (see also Fig. 11f). The combination of uncertainties between the two reanalyses complicates their intercomparison in the UTLS.

The differences between simulations with diabatic and kinematic vertical velocities are almost as large as the differences between ERA-Interim and ERA5 (see Fig. 11e). With kinematic vertical velocities, the upward transport in the BDC is as fast as with the diabatic transport scheme or even faster for levels between 400 K and 900 K. Therefore less air parcels can be found beween 400 K and 500 K compared to the diabatic vertical velocities. Additionally, the bias roughly resembles the bias found for the scenario with parameterised diffusion, and hence indicates an increased cross-isentropic vertical dispersion. With the help of the variance of the zeta coordinate, it can be shown that the cross-isentropic dispersion is still increased in ERA5 for kinematic calculations in comparison to the diabatic calculations (see Appendix Fig. C1). This result is similar to findings for ERA-Interim (Ploeger et al., 2010a). With kinematic velocities, increased air parcel numbers can be found closely above the tropopause as well, in comparison to the diabatic calculations. This possibly indicates increased transport across the tropopause from below. However, for the kinematic velocities higher numbers of air parcels are found in the troposphere, because the applied criteria for excluding air parcels from further transport (reaching the level where the zeta coordinate is zero) is not fulfilled. Therefore the increase of air parcels closely above the tropopause could be a consequence of higher air parcel numbers remaining in the troposphere as well.

https://doi.org/10.5194/gmd-2023-214
Preprint. Discussion started: 21 November 2023

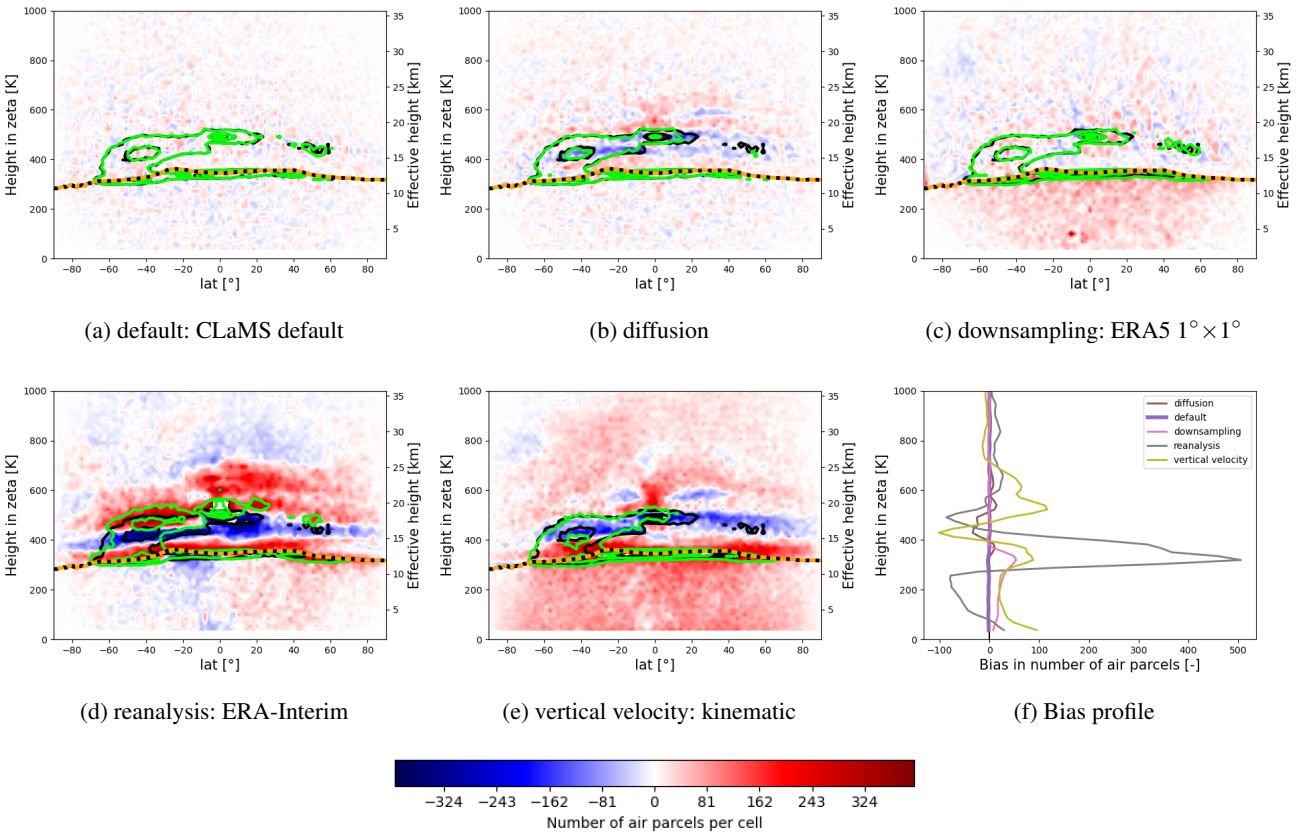

(a) default: CLaMS default (b) diffusion (c) downsampling: ERA5 1°×1°

(d) reanalysis: ERA-Interim (e) vertical velocity: kinematic (f) Bias profile

Figure 11. Zonal mean bias of the air parcel distributions after 90 days between the default MPTRAC scenario and a selected scenarios. Positive bias indicates lower frequency with the default MPTRAC scenario and higher frequency with the respective scenario. The orange dotted line is the 90 days average tropopause. The green contours show the 600, 1000 and 1400 air parcel number contours of the air parcel distributions for intercomparison with the scenarios (a) CLaMS default, (b) Diffusion, (c) downsampling: ERA5 1°×1°, (d) reanalysis: ERA-Interim and (e) vertical velocities: kinematic calculations. The black contours indicate same contour lines but for the MPTRAC default scenario. (f) displays a smoothed latitudinal average bias profile. The effective height is the average log-pressure height at a zeta level at the beginning of the calculations.

3.5 Conservation of dynamical tracers in the stratosphere

In the stratosphere, the potential temperature (θ) and the potential vorticity (PV) are approximately conserved. To assess the conservation of dynamical tracers in different scenarios with the newly implemented diabatic transport scheme in MPTRAC, Fig. 12a shows the 10-day evolution of the mean RTCE of the PV in the stratosphere, starting from 1 June 2016. Only air parcels with an initial height above 360 K, the approximated level of maximum convective outflow, are analysed. The mean conservation error after one day varies between 9% and 12%, depending on the scenario. After 10 days the mean RTCE increases to values between 22% and 27%. The differences between the different scenarios remain moderate, with slightly

https://doi.org/10.5194/gmd-2023-214
Preprint. Discussion started: 21 November 2023

Geoscientific Model Development Discussions
Open Access
EGU

improved PV conservation with ERA5 and diabatic velocities as implemented in MPTRAC. To estimate the significance of the improvement we compare it with the unresolved, parameterized sub-grid scale diffusion. The difference of the diabatic calculations with ERA5 compared to ERA5 $1° \times 1°$, the kinematic velocity scheme and ERA-Interim is almost as large as the difference between these scenarios with the scenario parameterised with sub-grid scale diffusion. These results exhibit slight improvements in conservation of PV with the newly implemented transport scheme in MPTRAC. Figure 12b shows the evolution of the conservation error of the potential temperature. The conservation is very similar for all scenarios except for the scenario with parameterised diffusion. Hence, in comparison to the uncertainties from parameterised diffusion, differences between scenarios are irrelevant.

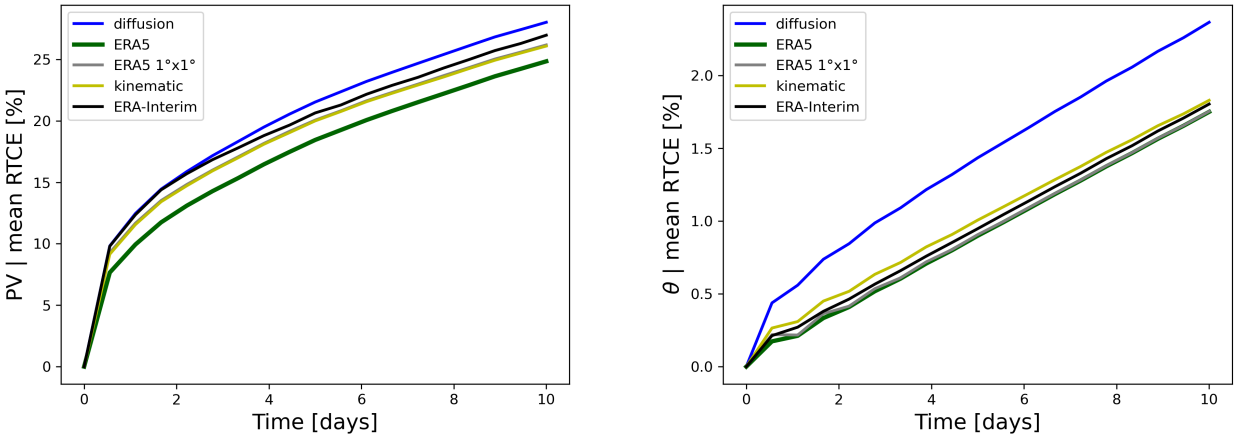

(a) PV (b) θ

Figure 12. Evolution of the mean RTCE of a) PV and b) theta for different scenarios within a 10 days period. All scenarios are driven with MPTRAC. See the scenarios in Table 1 between MPTRAC-default and MPTRAC-def-erai for further details. The starting date is 06/01/2016. Only air parcels with an initial altitude above 360 K are considered.

https://doi.org/10.5194/gmd-2023-214
Preprint. Discussion started: 21 November 2023

Geoscientific Model Development Discussions

4 Conclusions

In this study, we implemented a transport scheme based on hybrid zeta coordinates into the MPTRAC Lagrangian transport model. This work was mainly motivated by the intention to enable a transition from the CLaMS Lagrangian transport framework towards a code which is more suitable for upcoming HPC architectures. To assess the implementation of the zeta coordinate in MPTRAC, we conducted evaluations using approximately 1.4 million globally distributed air parcels in the troposphere and stratosphere, following an initialization method commonly employed in the CLaMS framework. Trajectory forward calculations were performed for the boreal summer of 2016. In our evaluation, we put the model differences in the context of various other uncertainty sources in Lagrangian transport calculations. Consequently, we present the model differences between CLaMS and MPTRAC within a hierarchy of uncertainties associated with Lagrangian transport models.

The key differences between the two Lagrangian models relate to their approach for interpolation of the driving meteorological data and the numerical integration scheme. Although models apply trilinear interpolations, CLaMS performs them directly in spherical coordinates, while MPTRAC performs them in Cartesian coordinates. As a default, CLaMS uses the classical fourth order Runge-Kutta scheme with 1800 s integration steps for numerical integration to run with feasible computational costs. MPTRAC employs the mid-point scheme with 180s integration time-steps. At a time-step of 180 s both integration schemes deliver very similar results, while the difference increases substantially when a time-step of 1800 s is chosen. This emphasizes the need to overcome computational limitations to run transport models with smaller time-step size. We also adjusted MPTRAC to fit better to the parameters and interpolation scheme as in the default CLaMS scenario, so that the agreement was slightly improved between the models (see "bestfit" scenarios). The residual differences between the models, are likely caused by remaining differences in the interpolation. For improved agreement, CLaMS and MPTRAC should use the identical Earth radius and use integration step sizes below 1800 s. Further alignment of the interpolations could achieve even better agreement.

Despite the conceptual model differences, we demonstrate that, for a period of 1 day, the discrepancy between CLaMS and MPTRAC air parcel vertical positions, which ranges from approximately 10^{-3}K to 10^{-2}K, is comparable to the combined internal uncertainties associated with different Earth radi, interpolation methods, numerical integration schemes and selected integration time-steps. These deviations are, at a minimum, around one order of magnitude smaller than the uncertainties arising from external sources, such as differences between reanalysis datasets (10^{-1}K to 1K), downsampling of the ERA5 reanalysis data (ranging from 10^{-1}K to 1K), and unresolved fluctuations of the wind fields (10^{-1}K to 1K). Thus, the analysis of the model differences indicates an excellent agreement of CLaMS and MPTRAC within the boundaries of known internal and external uncertainties. This holds also in the regions of most notable differences, including the troposphere and the winter stratosphere with the polar vortex.

We also estimated the uncertainty growth between the models and from external sources for 90 days. The vertical transport uncertainty remains low (less than around 1 K) for several weeks, in particular in the stratosphere. The transport deviation between the models is significantly smaller than the deviation caused by external sources of uncertainty for the entire 90 days time period. In particular, large uncertainty growth from variations of the vertical velocity (diabatic to kinematic) show that

https://doi.org/10.5194/gmd-2023-214
Preprint. Discussion started: 21 November 2023

Geoscientific Model Development Discussions

the implementation of the diabatic transport scheme into MPTRAC has significant impact on the transport of air parcels in comparison to the kinematic transport scheme.

Furthermore, the mean RTCE for PV and potential temperature were estimated for different MPTRAC scenarios. The mean RTCE of PV for air parcels above the 360K zeta level is between 22% and 27% for the MPTRAC model after 10 days. Diabatic calculations with ERA5 decrease the conservation error slightly (2-4%) in comparison to diabatic calculations with ERA-Interim, or calculations with ERA5 and kinematic vertical velocities. The mean RTCE is in agreement with values reported by Hoffmann et al. (2019) for kinematic calculations. Hoffmann et al. (2019) reported as well a decreased mean RTCE of PV with ERA5 relative to ERA-Interim. Only small differences with regard to the conservation of the potential temperature have been found here for the diabatic transport scenarios with ERA5 and ERA-Interim. This is in contrast to kinematic calculations of Hoffmann et al. (2019) who reported a reduced mean RTCE of the potential temperature with ERA5 for kinematic calculations in comparison to ERA-Interim. Some differences to Hoffmann et al. (2019) might as well be caused by differences in the initialization, which differs in year and initial air parcel distribution.

For global, long-term study of trace gases, the statistical distribution of air parcels in the UTLS, as opposed to individual trajectory errors, becomes more important. In their present configurations, both models distribute air parcels very similarly even after 90 days, supporting the hypothesis that the models provide similar long-term tracer fields. Accordingly, no biases in the air parcel distributions were found between the two models. In contrast, known external uncertainties caused significant biases in the trajectory calculations over the 90 day integration period. Differences between calculations with diabatic and kinematic vertical velocities are, even with ERA5, still on the order of reanalysis differences, further corroborating the implementation of the diabatic scheme into MPTRAC.

Furthermore, since model and internal uncertainties of the trajectory models are much smaller than uncertainties due to downsampling of ERA5 data, we conclude that using ERA5 $1^\circ \times 1^\circ$ for the sake of acceleration of computations has considerable side-effects. The bias is strongest in the troposphere for the ERA5 $1^\circ \times 1^\circ$ data. This stresses the important role of the spatiotemporal resolution of the global reanalysis fields, next to other improvements of the forecasts models and data assimilation schemes used to produce the reanalyses. Making Lagrangian models ready for operating with higher resolution meteorological data (as intended with MPTRAC) is fundamental to fully exploit the opportunities of next-generation reanalyses. Alternatively, applying better downsampling or data compression methods might be an option for future work.

Our results demonstrate that the largest uncertainty factors for Lagrangian transport calculations still arise from external sources, which is in agreement with prior findings (e.g. Stohl et al., 2001; Bowman et al., 2013; Hegarty et al., 2013; Angevine et al., 2014; Hoffmann et al., 2019), even with state-of-the-art models and reanalysis data. Given this hierarchy of uncertainties in the Lagrangian transport simulations, it is suggested that reduced accuracy due to linear interpolation or the application of the mid-point scheme in favour of speed-up of the calculations for runs based on higher resolution data is still a reasonable approach. Using linear interpolation is a common strategy in Lagrangian models (Bowman et al., 2013).

Ultimately, this evaluation shows that, with the newly implemented hybrid zeta coordinates, MPTRAC can replace CLaMS' trajectory module, without introducing any significant biases or other deviations. Thus MPTRAC can be coupled safely to global 3-dimension simulation with CLaMS including i.a. irreversible mixing and stratospheric chemistry in the future and

https://doi.org/10.5194/gmd-2023-214
Preprint. Discussion started: 21 November 2023

Geoscientific Model Development Discussions
Open Access
EGU

exploit the significant changes found with the high resolution ERA5 reanalysis combined with diabatic transport. The MPTRAC model is a suitable candidate for substituting CLaMS' trajectory calculations in HPC-based future applications.

Appendix A: Numerical stability analysis of the trajectory calculations

We use the Courant-Friedrichs-Lewy criterion to assess the stability of the trajectory calculations for different time-steps Δt (180 s and 1800 s) and horizontal grid resolution Δx (0.3°and 1°), horizontal windspeed u. The Courant-Friedrichs-Lewy number is defined as $\frac{u\Delta t}{\Delta x}$ and needs to be lower than 1 for stable integration conditions. We estimate the maximal velocity compatible with this restriction according to $v = \frac{\Delta x}{\Delta t}$. For 180 s time-steps we find velocities of around 185 ms^{-1} for 0.3°grids (around 617 ms^{-1} for 1.0°grids), which allows stable integration even at the location of highest velocities in the jet-streams. However for 1800 s time-steps the maximum velocity for stable integration is only 18.5 ms^{-1} for 0.3°grids, which is higher than the climatological average in many regions, but lower for the jet cores and daily extreme winds. For the 1.0°grid the maximum stable wind velocity is 61.7 ms^{-1} which is higher than the climatological zonal wind speeds, but might not be so under the most extreme conditions in jet streams. Additionally it has to be kept in mind that these velocities are upper limits that decrease with higher latitudes because the grid-size Δx will decrease as well.

Appendix B: Circulation in the UTLS

To clarify the differences in the circulation patterns during the 90 days integration period, Fig. B1 shows the boxwise averaged trajectories. With a grid (around $8° \times 32$ K) using the initial positions, air parcels have been sorted into groups. Bins with less than 100 air parcels are excluded. The average position of this groups of air parcels following them in time defines the box-wise average trajectory. Then, the vector is calculated, that connects the end point of the MPTRAC default scenario with the end point of the compared scenario.

https://doi.org/10.5194/gmd-2023-214
Preprint. Discussion started: 21 November 2023

Geoscientific Model Development Discussions
Open Access
EGU

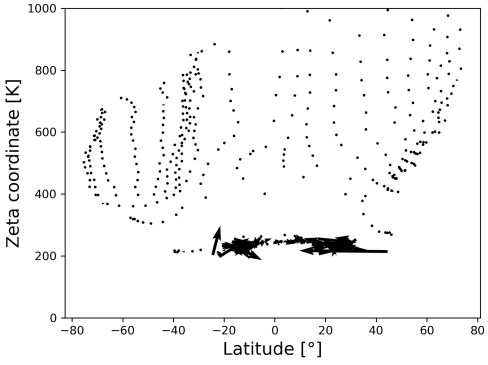

(a) default: CLaMS default

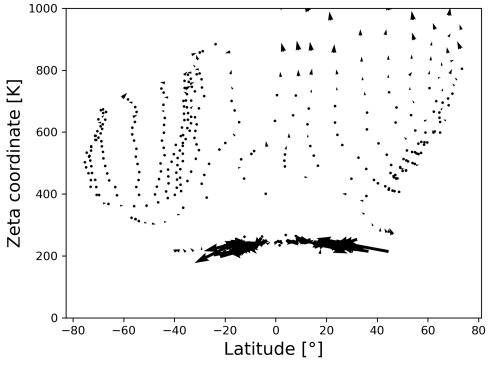

(b) diffusion

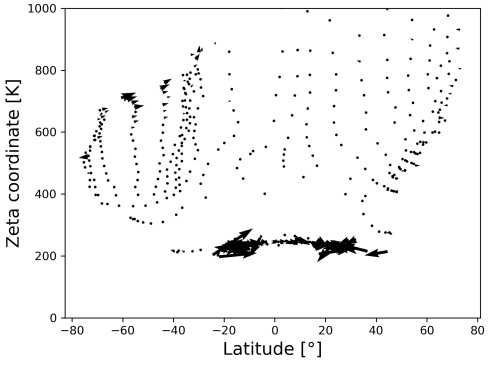

(c) downsampling: ERA5 $1^\circ \times 1^\circ$

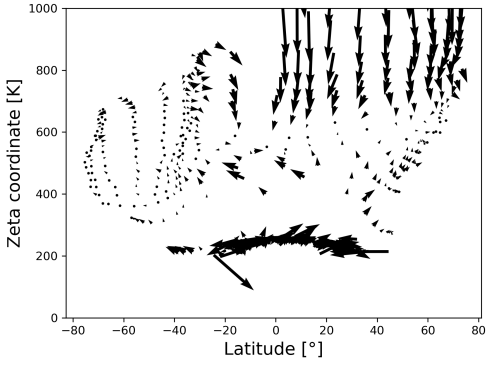

(d) reanalysis: ERA-Interim

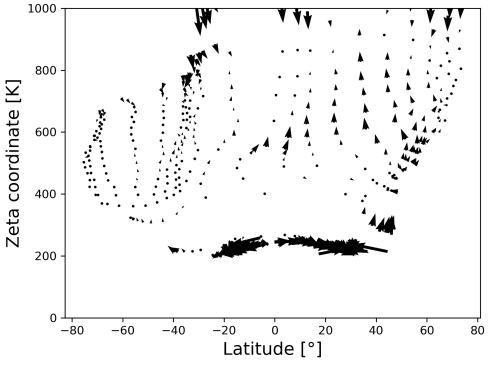

(e) vertical velocity: kinematic

Figure B1. Vector differences of end points of box wise averaged trajectories for the 90 days transport calculations in the UTLS and troposphere. The arrows indicate how the final MPTRAC-default positions have to be adjusted to agree with the respective scenario. Accordingly, they show the trajectory biases.

https://doi.org/10.5194/gmd-2023-214
Preprint. Discussion started: 21 November 2023

Geoscientific Model Development Discussions

Appendix C: Cross-isentropic dispersion of air parcels

The cross-isentropic dispersion of air parcels can be further quantified with the time variance of the potential temperature (Sparling et al., 1997; Ploeger et al., 2011). Fig. C1 shows the vertical profile of the variance of the zeta coordinate for all air parcels on different levels after 10 days. For levels higher than 360 K the zeta coordinate agrees with isentropic coordinates, i.e. potential temperatures (Pommrich et al., 2014). The kinematic calculations with ERA5 still have a higher dispersion in comparison to the diabatic calculations, however the dispersion of parameterised diffusion is much higher. There are small differences between the dispersion in the reanalysis ERA5 and ERA-Interim as well for the diabatic calculations. The two models agree highly with regard to the dispersion.

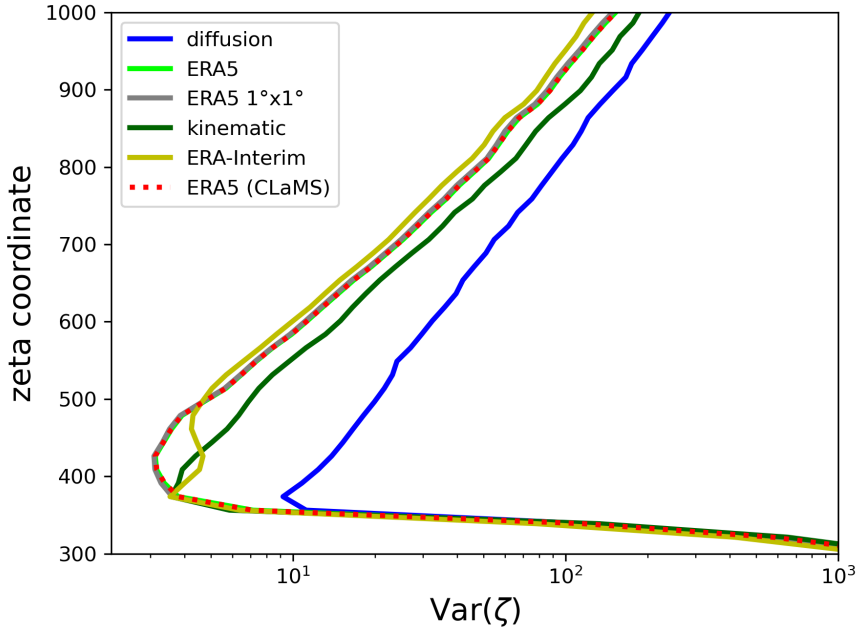

Figure C1. The variance of the zeta coordinate as a measure of the cross-isentropic transport.

Code and data availability. The CLaMS code can be accessed from the Jülich GitLab server: https://jugit.fz-juelich.de/clams/CLaMS (last access: 28 Oktober 2022). MPTRAC is made available under the terms and conditions of the GNU General Public License (GPL) version 3. New versions of MPTRAC are made available via the repository at https://github.com/slcs-jsc/mptrac (last access: 28 Oktober 2023). The diabatic transport scheme presented in this study is published in Release version 2.6 of MPTRAC (Hoffmann et al., 2023a). The exact model code, scripts, configuration files and initial data used for this study have been archived on Zenodo (Clemens, 2023).

https://doi.org/10.5194/gmd-2023-214
Preprint. Discussion started: 21 November 2023

Geoscientific Model Development Discussions

Author contributions. Conceptualization: J.C., L.H., B.V., S.G. and N.T.; Data curation: J.C., L.H. and N.T.; Formal analysis: J.C.; Funding acquisition: L.H. and B.V.; Methodology: J.C., L.H., B.V., S.G. and N.T.; Project administration: L.H. and B.V.; Resources: L.H., B.V., S.G. and N.T.; Software: J.C.; Supervision: L.H. and B.V.; Validation: J.C. and L.H.; Visualization: J.C.; Writing – original draft: J.C.; Writing - review & editing: J.C., L.H., B.V. and S.G.

Competing interests. The contact author has declared that neither they nor their co-authors have any competing interests.

Acknowledgements. This research has been supported by the Helmholtz Association of German Research Centres (HGF) through the Joint Lab Exascale Earth System Modelling (JL-ExaESM). We acknowledge the Jülich Supercomputing Centre for providing computing time and storage resources on the JUWELS supercomputer. Jan Clemens was partly funded by Helmholtz Interdisciplinary Doctoral Training in Energy and Climate Research (HITEC). We also thank the ECMWF for providing access to the ERA5 and ERA-Interim reanalysis data. We also acknowledge modern, AI based spelling software (DeepL, ChatGPT) which was used limited to check, correct and improve the language. We thank Paul Konopka and Felix Plöger for the discussion about results and methods.

https://doi.org/10.5194/gmd-2023-214
Preprint. Discussion started: 21 November 2023

Geoscientific Model Development Discussions

References

Angevine, W. M., Brioude, J., McKeen, S., and Holloway, J. S.: Uncertainty in Lagrangian pollutant transport simulations due to meteorological uncertainty from a mesoscale WRF ensemble, Geosci. Model Dev., 7, 2817–2829, https://doi.org/10.5194/gmd-7-2817-2014, 2014.

Bauer, P., Dueben, P. D., Hoefler, T., Quintino, T., Schulthess, T. C., and Wedi, N. P.: The digital revolution of Earth-system science, Nat. Comput. Sci., 1, 104–113, https://doi.org/10.1038/s43588-021-00023-0, 2021.

Bowman, K. P., Lin, J. C., Stohl, A., Draxler, R., Konopka, P., Andrews, A., and Brunner, D.: Input Data Requirements for Lagrangian Trajectory Models, Bull. Am. Meteorol. Soc., 94, 1051–1058, https://doi.org/10.1175/BAMS-D-12-00076.1, 2013.

Brinkop, S. and Jöckel, P.: ATTILA 4.0: Lagrangian advective and convective transport of passive tracers within the ECHAM5/MESSy (2.53.0) chemistry–climate model, Geosci. Model Dev., 12, 1991–2008, https://doi.org/10.5194/gmd-12-1991-2019, 2019.

Clemens, J.: Model code, processing scripts, initial and configuration data., https://doi.org/10.5281/zenodo.10050089, 2023.

Clemens, J., Vogel, B., Hoffmann, L., Griessbach, S., Thomas, N., Fadnavis, S., Müller, R., Peter, T., and Ploeger, F.: Identification of source regions of the Asian Tropopause Aerosol Layer on the Indian subcontinent in August 2016, EGUsphere, pp. 1–39, https://doi.org/10.5194/egusphere-2022-1462, 2023.

Dee, D. P., Uppala, S. M., Simmons, A. J., Berrisford, P., Poli, P., Kobayashi, S., Andrae, U., Balmaseda, M. A., Balsamo, G., Bauer, P., Bechtold, P., Beljaars, A. C. M., van de Berg, L., Bidlot, J., Bormann, N., Delsol, C., Dragani, R., Fuentes, M., Geer, A. J., Haimberger, L., Healy, S. B., Hersbach, H., Hólm, E. V., Isaksen, L., Kållberg, P., Köhler, M., Matricardi, M., McNally, A. P., Monge-Sanz, B. M., Morcrette, J.-J., Park, B.-K., Peubey, C., de Rosnay, P., Tavolato, C., Thépaut, J.-N., and Vitart, F.: The ERA-Interim reanalysis: configuration and performance of the data assimilation system, Q. J. R. Meteorol. Soc., 137, 553–597, https://doi.org/10.1002/qj.828, 2011.

Eluszkiewicz, J., Hemler, R. S., Mahlman, J. D., Bruhwiler, L., and Takacs, L. L.: Sensitivity of Age-of-Air Calculations to the Choice of Advection Scheme, J. Atmos. Sci., 57, 3185–3201, https://doi.org/10.1175/1520-0469(2000)057<3185:SOAOAC>2.0.CO;2, 2000.

Hegarty, J., Draxler, R. R., Stein, A. F., Brioude, J., Mountain, M., Eluszkiewicz, J., Nehrkorn, T., Ngan, F., and Andrews, A.: Evaluation of Lagrangian Particle Dispersion Models with Measurements from Controlled Tracer Releases, J. Appl. Meteorol. Climatol., 52, 2623–2637, https://doi.org/10.1175/JAMC-D-13-0125.1, 2013.

Hersbach, H., Bell, B., Berrisford, P., Hirahara, S., Horányi, A., Muñoz-Sabater, J., Nicolas, J., Peubey, C., Radu, R., Schepers, D., Simmons, A., Soci, C., Abdalla, S., Abellan, X., Balsamo, G., Bechtold, P., Biavati, G., Bidlot, J., Bonavita, M., De Chiara, G., Dahlgren, P., Dee, D., Diamantakis, M., Dragani, R., Flemming, J., Forbes, R., Fuentes, M., Geer, A., Haimberger, L., Healy, S., Hogan, R. J., Hólm, E., Janisková, M., Keeley, S., Laloyaux, P., Lopez, P., Lupu, C., Radnoti, G., de Rosnay, P., Rozum, I., Vamborg, F., Villaume, S., and Thépaut, J.-N.: The ERA5 global reanalysis, Q. J. R. Meteorol. Soc., 146, 1999–2049, https://doi.org/10.1002/qj.3803, 2020.

Hoffmann, L., Hertzog, A., Rößler, T., Stein, O., and Wu, X.: Intercomparison of meteorological analyses and trajectories in the Antarctic lower stratosphere with Concordiasi superpressure balloon observations, Atmos. Chem. Phys., 17, 8045–8061, https://doi.org/10.5194/acp-17-8045-2017, 2017.

Hoffmann, L., Günther, G., Li, D., Stein, O., Wu, X., Griessbach, S., Heng, Y., Konopka, P., Müller, R., Vogel, B., and Wright, J. S.: From ERA-Interim to ERA5: the considerable impact of ECMWF's next-generation reanalysis on Lagrangian transport simulations, Atmos. Chem. Phys., 19, 3097–3124, https://doi.org/10.5194/acp-19-3097-2019, 2019.

https://doi.org/10.5194/gmd-2023-214
Preprint. Discussion started: 21 November 2023

Hoffmann, L., Baumeister, P. F., Cai, Z., Clemens, J., Griessbach, S., Günther, G., Heng, Y., Liu, M., Haghighi Mood, K., Stein, O., Thomas, N., Vogel, B., Wu, X., and Zou, L.: Massive-Parallel Trajectory Calculations version 2.2 (MPTRAC-2.2): Lagrangian transport simulations on graphics processing units (GPUs), Geosci. Model Dev., 15, 2731–2762, https://doi.org/10.5194/gmd-15-2731-2022, 2022.

Hoffmann, L., Clemens, J., Griessbach, S., Haghighi Mood, K., Khosrawi, F., Liu, M., Lu, Y.-S., Sonnabend, J., and Zou, L.: Massive-Parallel Trajectory Calculations (MPTRAC) v2.6, https://doi.org/10.5281/zenodo.10067751, 2023a.

Hoffmann, L., Konopka, P., Clemens, J., and Vogel, B.: Lagrangian transport simulations using the extreme convection parameterization: an assessment for the ECMWF reanalyses, Atmos. Chem. Phys., 23, 7589–7609, https://doi.org/10.5194/acp-23-7589-2023, 2023b.

Konopka, P., Steinhorst, H.-M., Grooß, J.-U., Günther, G., Müller, R., Elkins, J. W., Jost, H.-J., Richard, E., Schmidt, U., Toon, G., and McKenna, D. S.: Mixing and ozone loss in the 1999–2000 Arctic vortex: Simulations with the three-dimensional Chemical Lagrangian Model of the Stratosphere (CLaMS), J. Geophys. Res., 109, https://doi.org/https://doi.org/10.1029/2003JD003792, 2004.

Konopka, P., Günther, G., Müller, R., dos Santos, F. H. S., Schiller, C., Ravegnani, F., Ulanovsky, A., Schlager, H., Volk, C. M., Viciani, S., Pan, L. L., McKenna, D.-S., and Riese, M.: Contribution of mixing to upward transport across the tropical tropopause layer (TTL), Atmos. Chem. Phys., 7, 3285–3308, https://doi.org/10.5194/acp-7-3285-2007, 2007.

Konopka, P., Tao, M., von Hobe, M., Hoffmann, L., Kloss, C., Ravegnani, F., Volk, C. M., Lauther, V., Zahn, A., Hoor, P., and Ploeger, F.: Tropospheric transport and unresolved convection: numerical experiments with CLaMS 2.0/MESSy, Geosci. Model Dev., 15, 7471–7487, https://doi.org/10.5194/gmd-15-7471-2022, 2022.

Li, D., Vogel, B., Müller, R., Bian, J., Günther, G., Ploeger, F., Li, Q., Zhang, J., Bai, Z., Vömel, H., and Riese, M.: Dehydration and low ozone in the tropopause layer over the Asian monsoon caused by tropical cyclones: Lagrangian transport calculations using ERA-Interim and ERA5 reanalysis data, Atmos. Chem. Phys., 20, 4133–4152, https://doi.org/10.5194/acp-20-4133-2020, 2020.

Liu, M., Hoffmann, L., Griessbach, S., Cai, Z., Heng, Y., and Wu, X.: Improved representation of volcanic sulfur dioxide depletion in Lagrangian transport simulations: a case study with MPTRAC v2.4, EGUsphere, pp. 1–29, https://doi.org/10.5194/egusphere-2022-1480, 2023.

Mahowald, N. M., Plumb, R. A., Rasch, P. J., del Corral, J., Sassi, F., and Heres, W.: Stratospheric transport in a three-dimensional isentropic coordinate model, J. Geophys. Res., 107, ACH 3–1–ACH 3–14, https://doi.org/https://doi.org/10.1029/2001JD001313, 2002.

McKenna, D. S., Grooß, J.-U., Günther, G., Konopka, P., Müller, R., Carver, G., and Sasano, Y.: A new Chemical Lagrangian Model of the Stratosphere (CLaMS) 2. Formulation of chemistry scheme and initialization, J. Geophys. Res., 107, ACH 4–1–ACH 4–14, https://doi.org/10.1029/2000JD000113, 2002a.

McKenna, D. S., Konopka, P., Grooß, J.-U., Günther, G., Müller, R., Spang, R., Offermann, D., and Orsolini, Y.: A new Chemical Lagrangian Model of the Stratosphere (CLaMS) 1. Formulation of advection and mixing, J. Geophys. Res., 107, ACH 15–1–ACH 15–15, https://doi.org/10.1029/2000JD000114, 2002b.

Ploeger, F., Konopka, P., Günther, G., Grooß, J.-U., and Müller, R.: Impact of the vertical velocity scheme on modeling transport across the tropical tropopause layer, J. Geophys. Res., 115, D03301, https://doi.org/10.1029/2009JD012023, 2010a.

Ploeger, F., Konopka, P., Günther, G., Grooß, J.-U., and Müller, R.: Impact of the vertical velocity scheme on modeling transport in the tropical tropopause layer, J. Geophys. Res., 115, https://doi.org/10.1029/2009JD012023, 2010b.

Ploeger, F., Fueglistaler, S., Grooß, J.-U., Günther, G., Konopka, P., Liu, Y. S., Müller, R., Ravegnani, F., Schiller, C., Ulanovski, A., and Riese, M.: Insight from ozone and water vapour on transport in the tropical tropopause layer (TTL), Atmos. Chem. Phys., 11, 407–419, https://doi.org/10.5194/acp-11-407-2011, 2011.

https://doi.org/10.5194/gmd-2023-214
Preprint. Discussion started: 21 November 2023

Ploeger, F., Diallo, M., Charlesworth, E., Konopka, P., Legras, B., Laube, J. C., Grooß, J.-U., Günther, G., Engel, A., and Riese, M.: The stratospheric Brewer–Dobson circulation inferred from age of air in the ERA5 reanalysis, Atmos. Chem. Phys., 21, 8393–8412, https://doi.org/10.5194/acp-21-8393-2021, 2021.

Pommrich, R., Müller, R., Grooß, J.-U., Konopka, P., Ploeger, F., Vogel, B., Tao, M., Hoppe, C. M., Günther, G., Spelten, N., Hoffmann, L., Pumphrey, H.-C., Viciani, S., D'Amato, F., Volk, C. M., Hoor, P., Schlager, H., and Riese, M.: Tropical troposphere to stratosphere transport of carbon monoxide and long-lived trace species in the Chemical Lagrangian Model of the Stratosphere (CLaMS), Geosci. Model Dev., 7, 2895–2916, https://doi.org/10.5194/gmd-7-2895-2014, 2014.

Rolph, G. D. and Draxler, R. R.: Sensitivity of Three-Dimensional Trajectories to the Spatial and Temporal Densities of the Wind Field, J. Appl. Meteorol. Climatol., 29, 1043–1054, https://doi.org/10.1175/1520-0450(1990)029<1043:SOTDTT>2.0.CO;2, 1990.

Rößler, T., Stein, O., Heng, Y., Baumeister, P., and Hoffmann, L.: Trajectory errors of different numerical integration schemes diagnosed with the MPTRAC advection module driven by ECMWF operational analyses, Geosci. Model Dev., 11, 575–592, https://doi.org/10.5194/gmd-11-575-2018, 2018.

Schoeberl, M. R. and Dessler, A. E.: Dehydration of the stratosphere, Atmos. Chem. Phys., 11, 8433–8446, https://doi.org/10.5194/acp-11-8433-2011, 2011.

Simmons, A. J., Burridge, D. M., Jarraud, M., Girard, C., and Wergen, W.: The ECMWF medium-range prediction models development of the numerical formulations and the impact of increased resolution, Meteor. Atmos. Phys., 40, 28–60, https://doi.org/10.1007/BF01027467, 1989.

Sparling, L. C., Kettleborough, J. A., Haynes, P. H., McIntyre, M. E., Rosenfield, J. E., Schoeberl, M. R., and Newman, P. A.: Diabatic cross-isentropic dispersion in the lower stratosphere, J. Geophys. Res., 102, 25 817–25 829, https://doi.org/10.1029/97JD01968, 1997.

Stohl, A.: Computation, accuracy and applications of trajectories—A review and bibliography, Atmo. Environ., 32, 947–966, https://doi.org/10.1016/S1352-2310(97)00457-3, 1998.

Stohl, A., Wotawa, G., Seibert, P., and Kromp-Kolb, H.: Interpolation Errors in Wind Fields as a Function of Spatial and Temporal Resolution and Their Impact on Different Types of Kinematic Trajectories, J. Appl. Meteorol. Climatol., 34, 2149–2165, https://doi.org/10.1175/1520-0450(1995)034<2149:IEIWFA>2.0.CO;2, 1995.

Stohl, A., Haimberger, L., Scheele, M. P., and Wernli, H.: An intercomparison of results from three trajectory models, Meteorol. Appl., 8, 127–135, https://doi.org/10.1017/S1350482701002018, 2001.

Stohl, A., Cooper, O. R., and James, P.: A Cautionary Note on the Use of Meteorological Analysis Fields for Quantifying Atmospheric Mixing, J. Atmos. Sci., 61, 1446–1453, https://doi.org/10.1175/1520-0469(2004)061<1446:ACNOTU>2.0.CO;2, 2004.

Vogel, B., Günther, G., Müller, R., Grooß, J.-U., and Riese, M.: Impact of different Asian source regions on the composition of the Asian monsoon anticyclone and of the extratropical lowermost stratosphere, Atmos. Chem. Phys., 15, 13 699–13 716, https://doi.org/10.5194/acp-15-13699-2015, 2015.

Vogel, B., Müller, R., Günther, G., Spang, R., Hanumanthu, S., Li, D., Riese, M., and Stiller, G. P.: Lagrangian simulations of the transport of young air masses to the top of the Asian monsoon anticyclone and into the tropical pipe, Atmos. Chem. Phys., 19, 6007–6034, https://doi.org/10.5194/acp-19-6007-2019, 2019.

Vogel, B., Volk, C. M., Wintel, J., Lauther, V., Müller, R., Patra, P. K., Riese, M., Terao, Y., and Stroh, F.: Reconstructing high-resolution in-situ vertical carbon dioxide profiles in the sparsely monitored Asian monsoon region, Commun. Earth Environ., 4, 72, https://doi.org/10.1038/s43247-023-00725-5, 2023a.

https://doi.org/10.5194/gmd-2023-214
Preprint. Discussion started: 21 November 2023

Vogel, B., Volk, M., Wintel, J., Lauther, V., Clemens, J., Grooß, J.-U., Günther, G., Hoffmann, L., Laube, J. C., Müller, R., Ploeger, F., and
745 Stroh, F.: Evaluation of vertical transport in the Asian monsoon 2017 from CO_2 reconstruction in the ERA5 and ERA-Interim reanalysis, EGUsphere, pp. 1–37, https://doi.org/10.5194/egusphere-2023-1026, 2023b.